Nutation Control During Precession of a Spin-Stabilized Spacecraft

by

Javin M. Taylor

Richard J. Donner

Vehbi Tasar

Technical Report CRL 73.6

December 1973

ELECTRICAL ENGINEERING RESEARCH

University of Missouri - Rolla

Rolla, Missouri 65401

NUTATION CONTROL DURING PRECESSION OF A SPIN-STABILIZED SPACECRAFT

by

Javin M. Taylor
Richard J. Donner
Vehbi Tasar

Department of Electrical Engineering
University of Missouri-Rolla
Rolla, Missouri 65401

Technical Report CRL 73.6

December 1973

NASA Grant No. NGR 26-003-069

ABSTRACT

The effects of precession thrust pulses and energy dissipation upon nutation of a spin-stabilized spacecraft are studied. Methods for controlling nutation during a precession maneuver are proposed and examined. In particular, a precession modulation control law is developed which uses precession thrust pulses to control nutation. Digital simulations show that precession control with separate nutation control is the fastest processing system; however, the precession modulation method is only fractionally slower while not requiring a separate nutation control system.

FOREWORD

The research covered by this report is supported by NASA Grant NGR 26-003-069, "Nutation Control During Precession of a Spin-Stabilized Spacecraft". The work was performed by Dr. Javin M. Taylor, Principal Investigator, Richard J. Donner, Master of Science Candidate in Electrical Engineering, and Vehbi Tasar, Master of Science Candidate in Computer Science, at the University of Missouri-Rolla under the supervision of Dr. Thomas W. Flatley, Earth Observations Systems & Systems Engineering Division, Space Applications and Technology Directorate, Goddard Space Flight Center.

This report represents the Semi-Annual Status Report for this project as required by NASA Provisions For Research Grants.

TABLE OF CONTENTS

LIST OF ILLUSTRATIONS

LIST OF ILLUSTRATIONS (cont.)

LIST OF TABLES

LIST OF SYMBOLS

I_x, I_y, I_z	moments of inertia about the principal axes of the spacecraft, x, y, and z
ω_x, ω_y, ω_z	angular velocities about axes of the spacecraft
$\omega(t)$	the transverse angular rate
ω_0	the magnitude of the transverse angular rate at t_0
ϕ_0	the angle at the start of a thrust pulse
t_0	the time at the start of a thrust pulse
t_1	the time at end of a thrust pulse
$\Delta\phi$	the angular duration of the thrust pulse
N	the complex torque
N_0	the magnitude of the torque
λ	the angular location of the thruster from the spacecraft y axis
Ω	the nutation frequency
Δt	duration of thrust pulse
τ	energy dissipation time constant
T	period of spin cycle
T_n	period of nutation cycle
$\Delta\omega p$	change in nutation magnitude due to thrust pulse
δ	the total angle that spans those values of ϕ_0 for which nutation is reduced
σ	ratio of spin axis inertia to transverse inertia
H	total angular momentum

I. INTRODUCTION

A spin-stabilized spacecraft requires a precession maneuver before reaching its final orbit. This maneuver is necessary to correctly align the line of action of the thruster that will be used for injection into the final orbit. This thruster is aligned with a spacecraft fixed spin axis which ideally points in the same direction as the angular momentum vector of the spinning spacecraft. However, for spacecraft spinning about the minimum inertia axis, this ideal case never exists. As a result, some components of the total angular momentum exist along axes perpendicular to the spin axis. These components are characterized by the transverse angular rate or nutation. Since the continual increase of nutation will eventually cause the spacecraft to spin about the maximum inertia axis, it is necessary to control this instability by holding the nutation below some acceptable threshold level.

Nutation can be affected by two conditions during a precession maneuver. The first is the sequence of precession thrust pulses which is capable of either increasing or decreasing the amount of nutation. The second is energy dissipation which will always increase the nutation of a spacecraft spinning about the minimum inertia axis.

Succeeding sections will discuss various aspects of nutation control during a precession maneuver. Section II briefly describes the basic nutation theory. Section III discusses the instability

of nutation during precession because of energy dissipation and nutation control through use of a separate system. In section IV two precession control laws that concurrently control nutation are presented and contrasted. Conclusions and recommendations for further study are given in section V.

II. NUTATION THEORY

Spin-stabilized spacecraft have their Cartesian axes along the principal inertia axes with the origin at the center of mass of the spacecraft. These moments of inertia are labeled I_x, I_y, I_z and are along the x, y, z axes respectively. The angular velocities are ω_x, ω_y, and ω_z. Generally the angular velocity of the spin axis is considered to be constant and the equations describing the dynamical system are simplified accordingly. Here ω_x is considered the spin velocity. Thus, the angular velocities ω_y and ω_z are considered the transverse angular velocities and indicate the amount of nutation present.

Previous nutation control studies by Grasshoff [1] and Taylor [2] form the basis for this paper. The result of their studies used herein is to characterize the transverse angular rate or nutation, $\omega(t)$, as the solution to the complex differential equation

$$\dot{\omega}(t) + i\Omega\omega(t) = N \tag{1}$$

where Ω is the nutation frequency. The applied torque due to thrust pulses is related to

$$N = N_0 e^{i\lambda} \tag{2}$$

where N_0 is a constant and λ is the angle measured ccw from the y axis. Derivation of equation (1) is described in Appendix D.

The homogeneous solution to (1) is given by

$$\omega(t) = \omega(t_0)e^{-i\Omega t}. \tag{3}$$

Thus, $\omega(t)$ is a vector that rotates clockwise in the complex plane with a frequency Ω. The complete solution to (1) is given by

$$\omega(t_1) = \omega(t_0)e^{-i\Omega(t_1 - t_0)} + \frac{N_0 e^{i\lambda}}{i\Omega}\left(1 - e^{-i\Omega(t_1 - t_0)}\right) \tag{4}$$

or

$$\omega(t_1) = \omega(t_0)e^{-i\Omega(t_1 - t_0)} + \frac{2N_0}{\Omega}\sin\left(\frac{\Omega(t_1 - t_0)}{2}\right)e^{i\left[\lambda - \frac{\Omega}{2}(t_1 - t_0)\right]} \tag{5}$$

It is noted that

$$\omega(t_0) = \omega_0 e^{-i\Omega t_0} \tag{6}$$

where

$$\omega_0 = \left|\omega(t_0)\right| \tag{7}$$

and

$$e^{-i\Omega t_0} = \angle\omega(t_0) \tag{8}$$

at $t = t_0$. The zero angle reference being taken as the y axis. To

show ω_0 with non-zero initial phase equation (5) can be rewritten as

$$\omega(t_1) = \omega_0 e^{-i\phi_0} e^{-i\Delta\phi} + \frac{2N_0}{\Omega} \sin(\frac{\Delta\phi}{2}) e^{i(\lambda - \frac{\Delta\phi}{2})} \tag{9}$$

where

$$\Delta\phi = \Omega(t_1 - t_0) \tag{10}$$

and

$$\phi_0 = \Omega t_0. \tag{11}$$

The components of equation (9) are shown in Figure 1. The larger circle centered at the origin is the locus of the initial transverse velocity vector. The smaller circle, or thrust lobe, tangent to the origin is the locus of the end of the thrust vector. The thrust lobe is situated as shown because of the value of λ. This value is a constant π for all discussions to follow herein.

The resultant vector $\omega(t_1)$ is a function of the variables ϕ_0, the angle at which the thrust pulse started; $\Delta\phi$, the duration of the thrust pulse; and m, the ratio of the thrust lobe radius to the nutation circle radius as given by the equation

$$m = \frac{N_0}{\Omega} \frac{1}{\omega_0} . \tag{12}$$

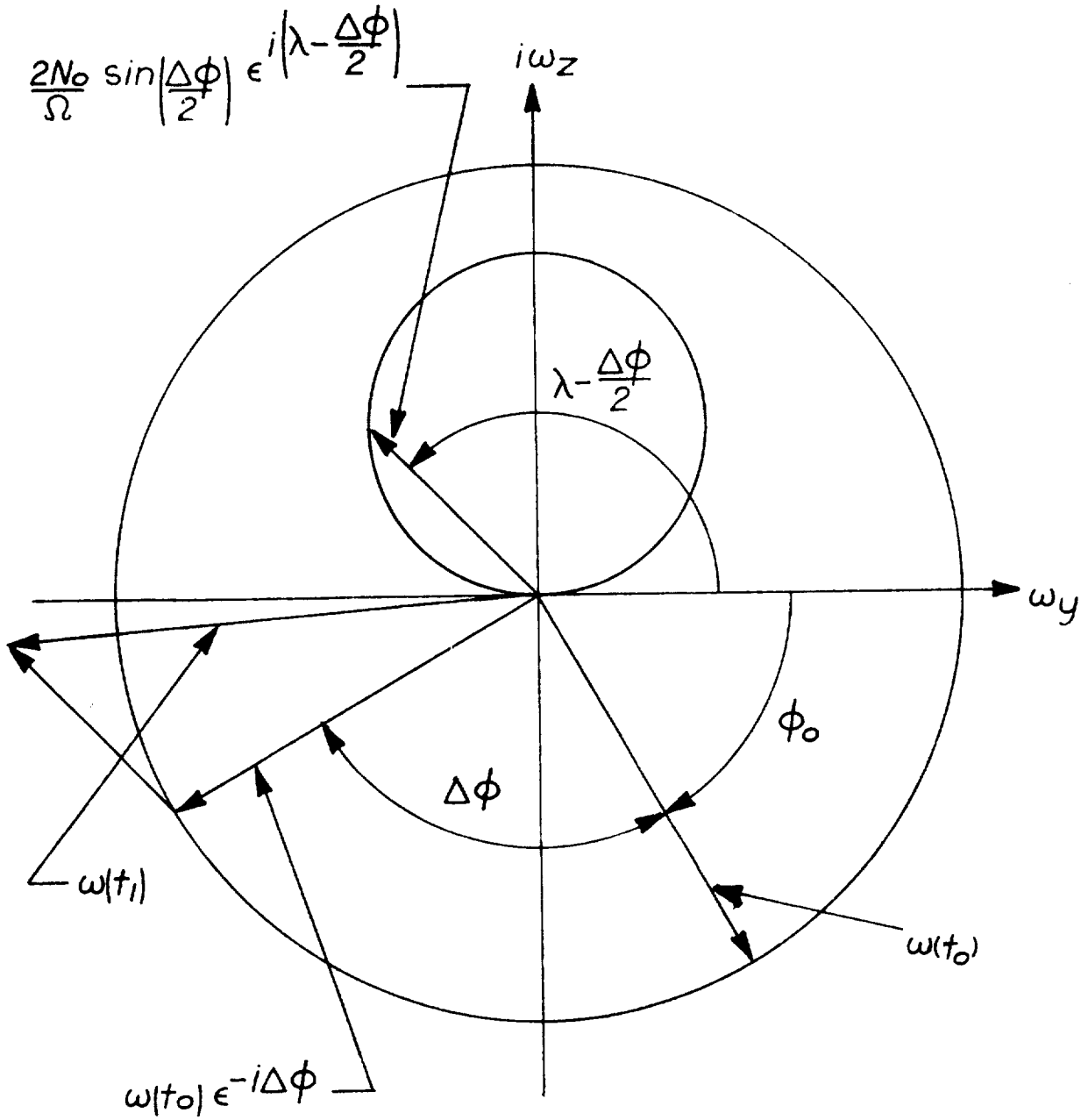

Figure 1. Nutation Circle and Precession Lobe

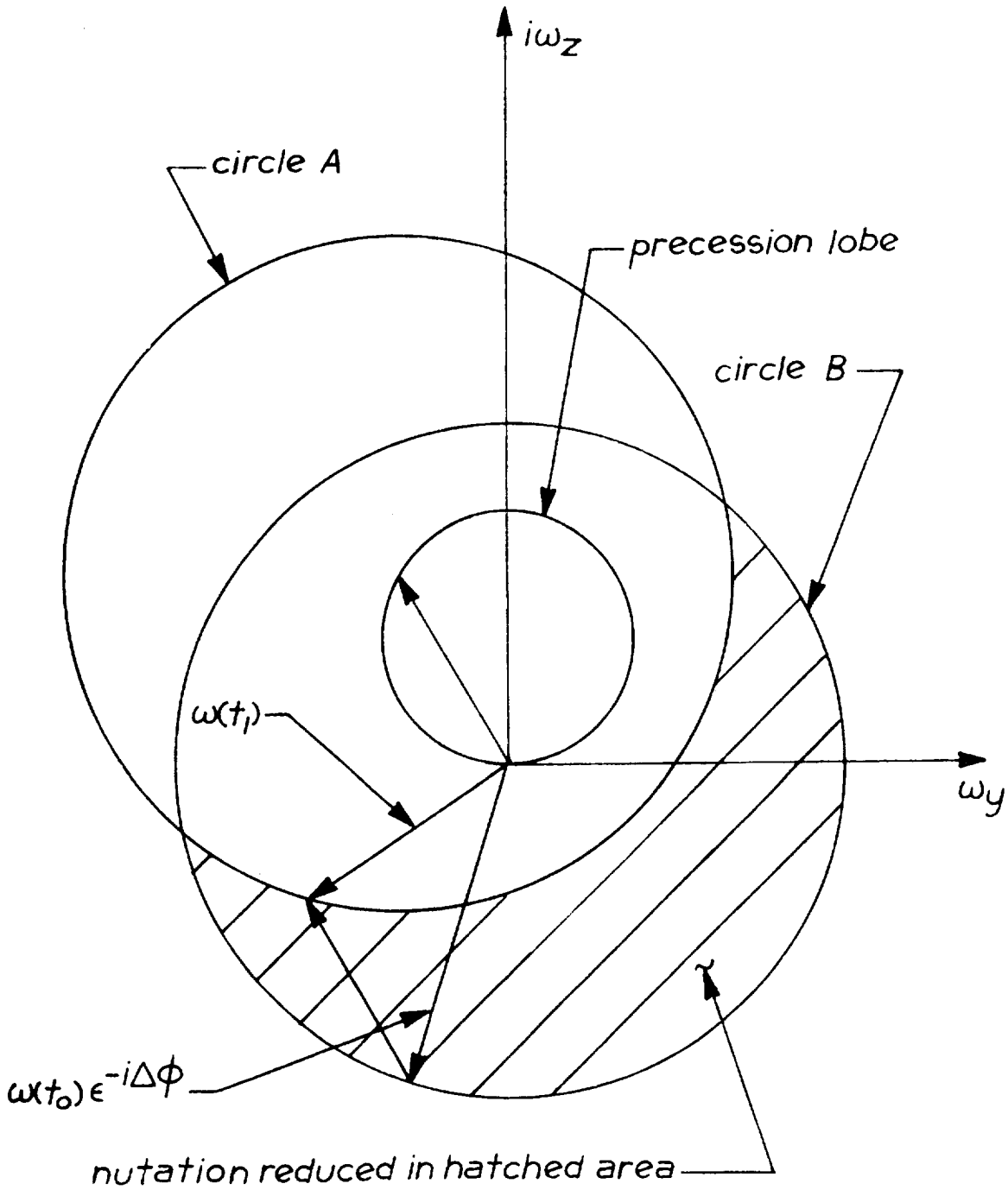

Figure 2. Nutation Reduction Area

In Figure 2 the interaction of these variables as they affect the result $\omega(t_1)$ is demonstrated. The circle A with its center at the tip of the vector $\frac{2N_0}{\Omega} \sin(\frac{\Delta\phi}{2}) e^{i(\lambda - \frac{\Delta\phi}{2})}$ describes the locus of the end of the vector $\omega(t_1)$ as a function of ϕ_0, the angle at the start of a given thrust pulse. The interpretation of Figure 2 is that when the distance from the origin of the coordinate system, at the center of circle B, to the circle A is less than ω_0 the nutation is reduced. Appendix A contains a discussion of the determination of the angle ϕ_0 for a given $\omega(t_1)$.

This section has described nutation effects caused by a single thruster. The same thruster can also be used to precess a spin-stabilized spacecraft. For short duration thrust pulses, precession is given by the simple relation $\Delta H/H$.

III. NUTATION DURING AN UNMODIFIED PRECESSION MANEUVER

In the context of this paper an unmodified precession maneuver is defined as a maneuver in which the precession thruster control signal is a sequence of pulses of duration Δt occurring every T seconds where T is the spin cycle period. Figure 3 shows such a sequence of pulses.

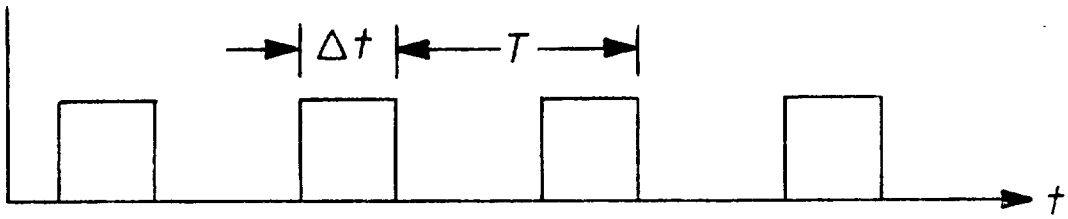

Figure 3. Precession Pulse Sequence

As was seen in section II, thrust pulses can either increase or decrease the nutation of a spin stabilized spacecraft. A previous study by Taylor [3] shows that for zero energy dissipation nutation is bounded and periodic due to changes caused by precession pulses. The following discussion examines the bound on the nutation during unmodified precession with energy dissipation present.

Equation (1) can be modified to include energy dissipation as follows

$$\dot{\omega}(t) + \left(-\frac{1}{\tau} + i\Omega\right)\omega(t) = N \tag{13}$$

where

τ = energy dissipation time constant. (14)

Making a notation simplification, (13) becomes

$$\dot{\omega}(t) + q\,\omega(t) = N \tag{15}$$

where

$$q = -\frac{1}{\tau} + i\omega \tag{16}$$

The solution to (15) is

$$\omega(t) = \omega(t_0)e^{-q(t - t_0)} + \frac{N}{q}(1 - e^{-q(t - t_0)}), \quad t_0 \leq t \leq \Delta t \tag{17}$$

$$\omega(t) = \omega(t_0)e^{-q(t - t_0)} + \frac{N}{q}(1 - e^{-q\Delta t})e^{-qt} \quad \Delta t < t \leq T \tag{18}$$

with Δt and T equal to the duration and period of the precession pulses respectively. Setting $t_0 = 0$, $t = T$, (18) becomes

$$\omega[T] = \omega[0]e^{-qT} + \frac{N}{q}(1 - e^{-q\Delta t})e^{-qT} \tag{19}$$

or

$$\omega[T] = \omega[0]e^{-qT} + F \tag{20}$$

where

$$F = \frac{N}{q}(1 - e^{-q\Delta t})e^{-qT} \tag{21}$$

Now, looking at solutions at t = 2T, ..., t = kT,

$$\omega[2T] = \omega[T]e^{-qT} + F \tag{22}$$

$$\vdots$$

$$\omega[kT] = \omega[(k-1)T]e^{-qT} + F \tag{23}$$

it is seen that (23) is a first order difference equation for the transverse angular rate at kT as a function of the transverse angular rate at (k-1)T. This first order difference equation is solved by use of the z-transform. The z-transform of (23) is given by

$$Z[\omega[kT]] = Z[\omega[(k-1)T]e^{-qT}] + Z[F] \tag{24}$$

$$W(z) = \omega[0] + z^{-1}e^{-qT}W(z) + \frac{F}{1 - z^{-1}} . \tag{25}$$

Solving for W(z)

$$W(z) = \frac{\omega[0]}{1 - e^{-qT}z^{-1}} + \frac{F}{(1 - e^{-qT}z^{-1})(1 - z^{-1})} \tag{26}$$

which upon expansion becomes

$$W(z) = \frac{\omega[0]}{1 - e^{-qT}z^{-1}} + \frac{F}{(1 - e^{-qT}z^{-1})(1 - e^{qT})} + \frac{F}{(1 - z^{-1})(1 - e^{-qT})} . \tag{27}$$

The inverse z-transform yields

$$Z^{-1}[W(z)] = \omega[nT] = \omega[0]e^{-qnT} + \frac{Fe^{-qnT}}{1 - e^{qT}} + \frac{F}{1 - e^{-qT}} . \tag{28}$$

Algebraic manipulation yields

$$\omega[nT] = \omega[0]e^{-qnT} + F\frac{1 - e^{-q(n+1)T}}{1 - e^{-qT}} \tag{29}$$

or

$$\omega[nT] = \omega[0]e^{-qnT} + C(1 - e^{-q(n+1)T}) \tag{30}$$

where

$$C = \frac{F}{1 - e^{-qT}} \tag{31}$$

is a phasor of constant angle and magnitude. Rearranging (30) as follows

$$\omega[nT] = (\omega[0] - Ce^{-qT})e^{-qnT} + C \tag{32}$$

it is evident that $\omega[nT]$ is bounded only if

$$\omega[0] = Ce^{-qT} \tag{33}$$

since e^{-qnT} is unbounded. Rewriting (32) with q replaced by (16)

$$\omega[nT] = Be^{\mu nT}e^{-i\Omega nT} + C \tag{34}$$

and

$$B = \omega[0] - Ce^{-qT} \tag{35}$$

clearly shows an unstable spiral offset from the origin of the coordinate system by the amount of the vector addition of B and C. This spiral is shown in Figure 4a.

In Figure 4b the nutation magnitude envelope and precession angle envelope are shown as a function of time. For some time, $T_{Critical}$, the nutation becomes so large as to make the definition of the direction of the spin axis meaningless for all practical purposes.

If a precession maneuver is to be successful the nutation must be limited to an acceptable value. Figure 5b shows the possible results for a separate nutation control system output ORed with the precession thrust command signal as shown in Figure 5a. Nutation control systems as described in [1] and [2] would meet this requirement. When a threshold value of nutation is reached the system operates until the nutation is reduced sufficiently. The times when the nutation control is active are labeled T_1, T_2, on the t axis of Figure 5b. A system like this will control the nutation build-up but has the disadvantage of complexity. It requires a precession control system and an independent nutation control.

The Figure 5b is only a generalized example of such a precession-nutation control system as shown in Figure 5a. Results of digital computer simulations for a specific spacecraft are shown in Appendix B.

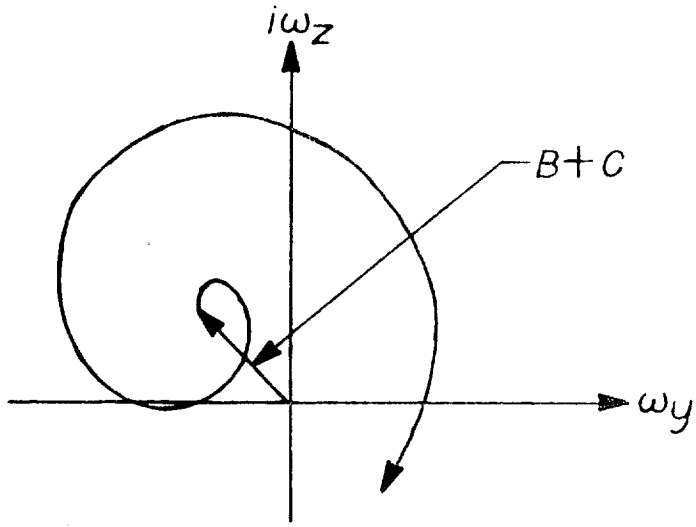

Figure 4a. Instability of Nutation Oscillation

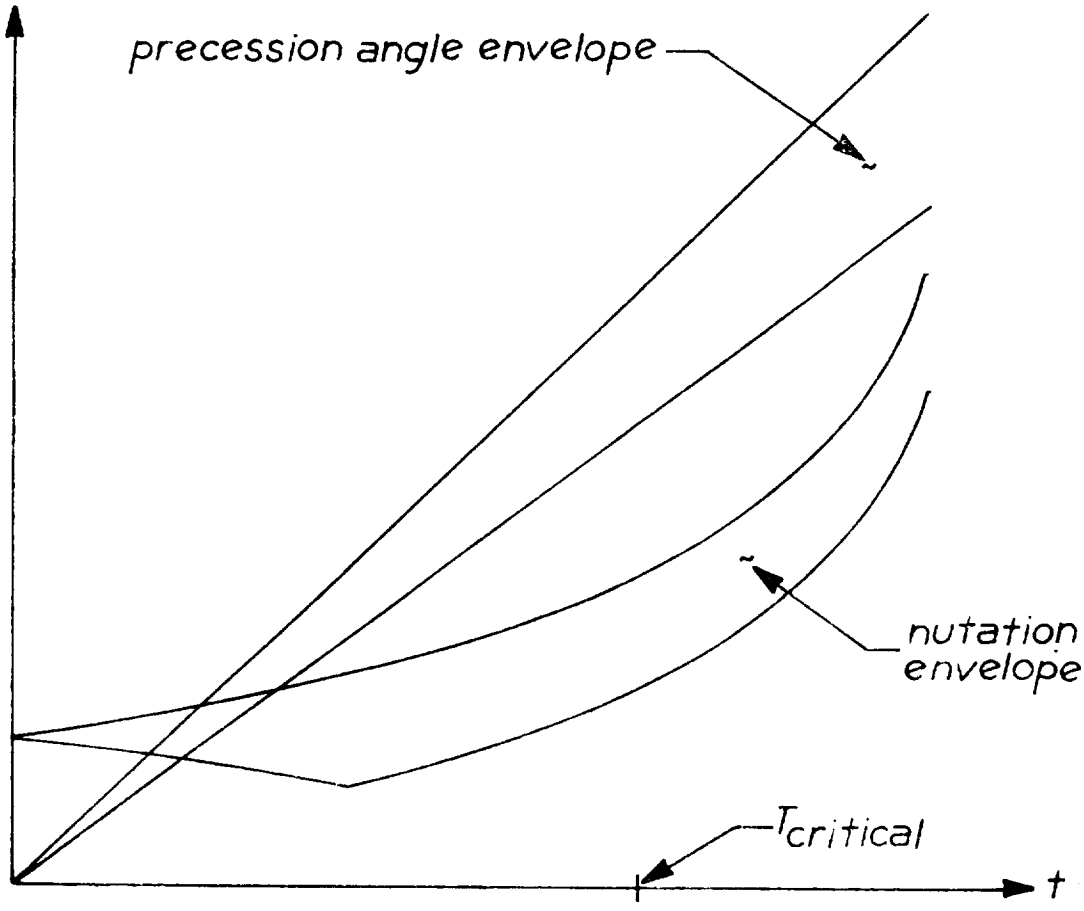

Figure 4b. Precession Angle Uncertainty and Instability of Nutation Oscillation

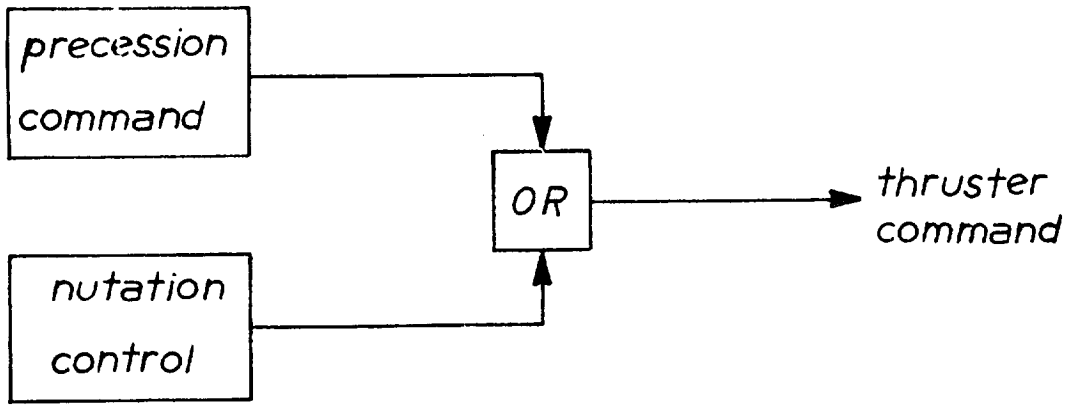

Figure 5a. Precession-Nutation Control Schematic

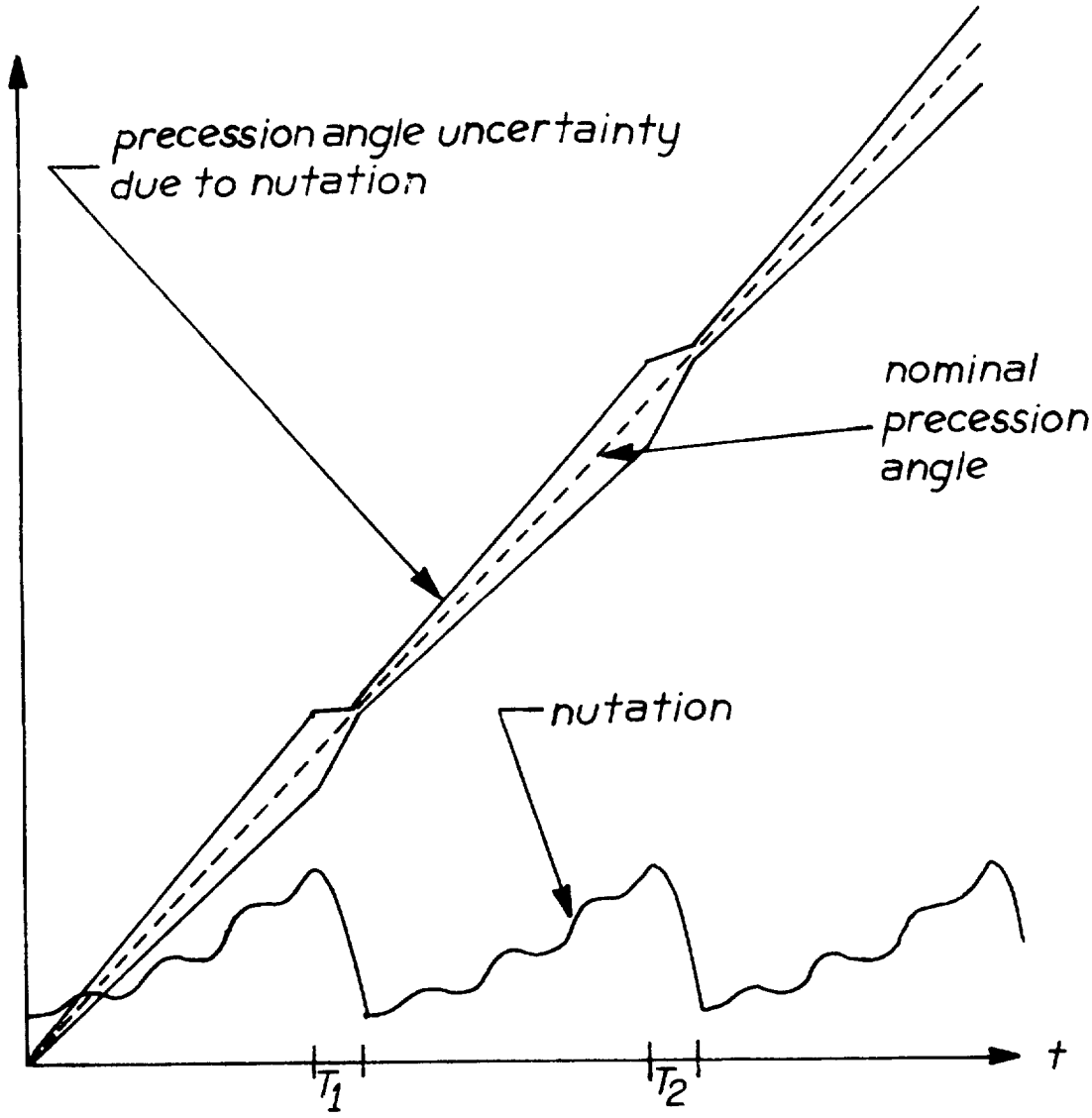

Figure 5b. Control System Operation

IV. MODULATED PRECESSION

Section III demonstrated that a precession maneuver could be carried out successfully if the nutation build-up was controlled by a separate nutation control system. This nutation control signal was ORed with the precession command. In that configuration an independent nutation control was used to suppress the negative effects of both the precession thrusting sequence and the energy dissipation. This section demonstrates that by modulating the precession sequence with a gating function the precession pulses themselves can be used to control nutation concurrently with the implementation of the precession maneuver. Figure 6 shows a schematic for such a system.

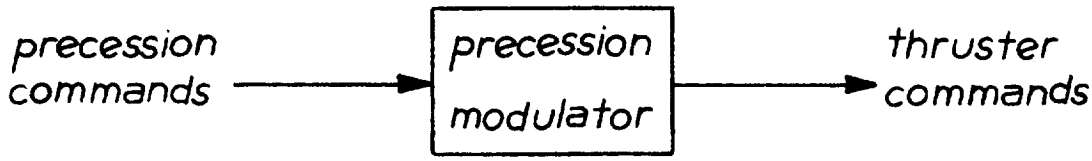

Figure 6. Precession Modulator System

The effects of precession pulses upon nutation as functions of several variables are analyzed in the following. The starting point is equation (9) which is repeated here for convenience.

$$\omega(t_1) = \omega_0 e^{-i\phi_0} e^{-i\Delta\phi} + \frac{2N_0}{\Omega} \sin(\frac{\Delta\phi}{2}) e^{i(\lambda - \frac{\Delta\phi}{2})} \tag{36}$$

Expanding $\omega(t_1)$ into sine and cosine functions and grouping the real and imaginary parts separately the following result is obtained.

$$\omega(t_1) = \omega_0 \cos(\phi_0 + \Delta\phi) + \frac{2N_0}{\Omega} \sin(\frac{\Delta\phi}{2})\cos(\lambda - \frac{\Delta\phi}{2}) + i\left[\frac{2N_0}{\Omega} \sin(\frac{\Delta\phi}{2})\sin(\lambda - \frac{\Delta\phi}{2}) - \omega_0 \sin(\phi_0 + \Delta\phi)\right] \tag{37}$$

What is sought at this point is an expression for the magnitude $|\omega(t_1)|$. Since

$$|\omega(t_1)|^2 = \omega(t_1)\omega(t_1)^* \tag{38}$$

where $\omega(t_1)^*$ is the complex conjugate of $\omega(t_1)$, then

$$|\omega(t_1)| = (\omega(t_1)\omega(t_1)^*)^{1/2}. \tag{39}$$

First $|\omega(t_1)|^2$ is derived by carrying out the multiplication indicated in (38), collecting terms, and making appropriate trigonometric substitutions. The result is

$$|\omega(t_1)|^2 = \omega_0^2 + \frac{4N_0^2}{\Omega^2} \sin^2(\frac{\Delta\phi}{2}) + \frac{4N_0}{\Omega} \omega_0 \sin(\frac{\Delta\phi}{2})(\cos(\phi_0 + \lambda + \frac{\Delta\phi}{2})) \tag{40}$$

The function $|\omega(t_1)|$ is now known in terms of ω_0 and several other variables.

Let a new function be defined as

$$\Delta\omega_p = |\omega(t_1)| - |\omega(t_0)| = |\omega(t_1)| - \omega_0. \tag{41}$$

This function describes the change in $\omega(t)$, the nutation, due to precession between the times t_0 and t_1. For the following discussion the variables $\Delta\phi$ and λ are constants and the function

$$\Delta\omega_p = f(\phi_0) \tag{42}$$

is studied. Equation (41) is now rewritten in its complete form which is

$$\Delta\omega_p = \left[\omega_0^2 + \frac{4N_0^2}{\Omega^2}\sin^2(\frac{\Delta\phi}{2}) + \frac{4N_0}{\Omega}\omega_0 \sin(\frac{\Delta\phi}{2})(\cos(\phi_0 + \lambda + \frac{\Delta\phi}{2}))\right]^{1/2} - \omega_0 \tag{43}$$

Since $\Delta\omega_p$ is to be used to control the nutation which would otherwise increase, those values of ϕ_0 for which

$$0 \geq \Delta\omega_p = f(\phi_0) \tag{44}$$

holds true will be determined. Clearly, from (43) if the condition of (44) is to be met then

$$0 \geq \frac{4N_0^2}{\Omega^2}\sin^2(\frac{\Delta\phi}{2}) + \frac{4N_0}{\Omega}\omega_0 \sin(\frac{\Delta\phi}{2})(\cos(\phi_0 + \lambda + \frac{\Delta\phi}{2})). \tag{45}$$

It should be noted at this point if

$$\Delta\phi = n2\pi, \quad n = 0,1,2,3,..... \tag{46}$$

then no net effect on precession can be obtained. Therefore, only those values of $\Delta\phi$ for which

$$0 < \Delta\phi < 2\pi \tag{47}$$

will be considered. Equation (45) can now be simplified to

$$-\frac{N_0}{\Omega}\left(\frac{1}{\omega_0}\right)\sin\left(\frac{\Delta\phi}{2}\right) \geq \cos\left(\phi_0 + \lambda + \frac{\Delta\phi}{2}\right) \tag{48}$$

which becomes

$$\arccos\left[-\frac{N_0}{\Omega}\left(\frac{1}{\omega_0}\right)\sin\left(\frac{\Delta\phi}{2}\right)\right] - \lambda - \frac{\Delta\phi}{2} \geq \phi_0. \tag{49}$$

Making a substitution based on (12) yields

$$\arccos\left[-m \sin\left(\frac{\Delta\phi}{2}\right)\right] - \lambda - \frac{\Delta\phi}{2} \geq \phi_0. \tag{50}$$

A useful change in (50) in terms of making computations is detailed in the following. Let

$$\cos\psi = -m \sin\left(\frac{\Delta\phi}{2}\right). \tag{51}$$

Because of (47) the range of $\cos\psi$ will be

$$0 > \cos\psi \geq -1 \tag{52}$$

which is shown in Figure 7.

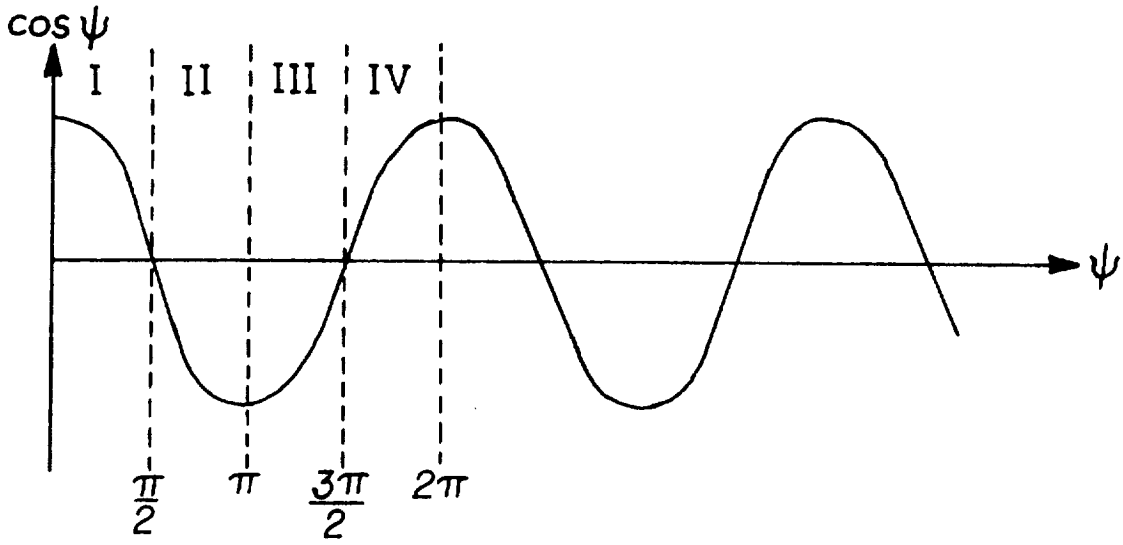

Figure 7. Determination of Quadrant for ψ

Equation (52) is satisfied for

$$\frac{\pi}{2} < \psi \leq \pi \text{ and } \frac{3\pi}{2} > \psi \geq \pi. \tag{53}$$

Because of this, (50) can be rewritten as

$$\arccos[-m \sin(\tfrac{\Delta\phi}{2})]_{II} - \lambda - \frac{\Delta\phi}{2} \leq \phi_0 \leq \arccos[-m \sin(\tfrac{\Delta\phi}{2})]_{III} - \lambda - \frac{\Delta\phi}{2} \tag{54}$$

where $\arccos[\cdot]_{II}$ and $\arccos[\cdot]_{III}$ refer to angles in the II and III quadrants respectively in Figure 7. Appendix C gives graphical results for equation (54) as the variables m, ϕ_0, and $\Delta\phi$ assume various values.

The time between the occurrence of pulses in the modulated precession pulse sequence determines the total amount of time required to complete the precession maneuver and the increase of

nutation between nutation reduction. Figure 8 provides a graphical basis for a discussion of this time between modulated precession pulses.

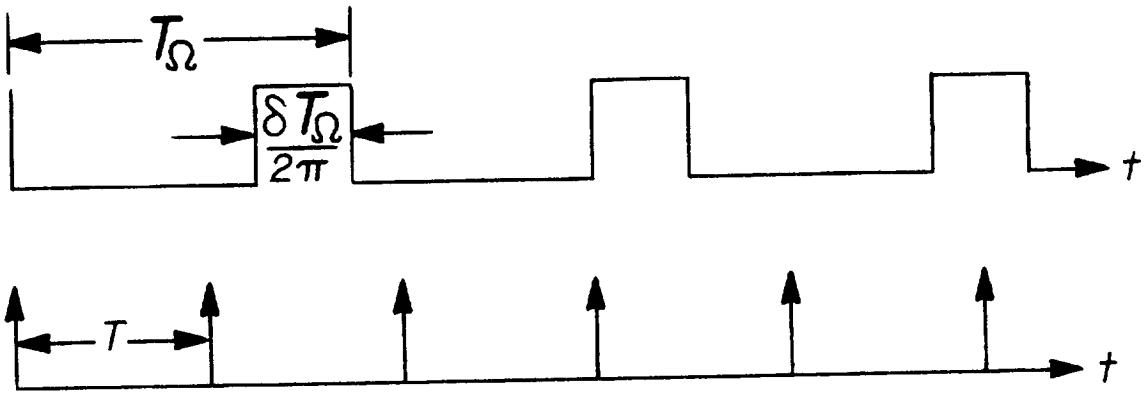

Figure 8. Time Between Modulated Pulses

In Figure 8 the top line represents the precession modulator gating function. The width of the gate is $\frac{\delta T_\Omega}{2\pi}$ where δ,

$$0 \leq \delta \leq \pi, \tag{55}$$

is a function of m and $\Delta\phi$ as shown in Appendix C. The time for one nutation cycle is T_Ω. The sequence of vectors in the second line represents the leading edge of each precession pulse command coming into the modulator. The spacing of these vectors is T, the spin cycle period. For some time kT the following equation is valid.

$$nT_\Omega(1 - \frac{\delta}{2\pi}) \leq kT \leq nT_\Omega \tag{56}$$

where

$$n = 1,2,3,.....$$

$$k = 1,2,3,.....$$

The physical meaning of Figure 8 is that when a leading edge vector occurs in a gate window that precession pulse is used.

Equation (56) does not permit a general analytic result for the values of n and k; however, Table 1 carries the results of a specific case.

Gate width in % of T_Ω	Maximum precession pulse separation in spin periods
50	3
45.5	3
41.8	3
36.4	3
31.8	5
27.3	5
22.8	5
18.2	5
16.6	8
9.1	13
4.6	23

Table I. Maximum Precession Pulse Separation for $T_\Omega/T = 1.656$

From Table 1 it is clearly seen that as the value of δ decreases the time between pulses becomes longer.

One reason for the foregoing analysis is to determine if the condition can exist in which the time between gated precession pulses is so great that the nutation increase due to energy dissipation is greater than the nutation that can be removed by a precession pulse. A condition such as this could result in an unstable situation of the type discussed in section III. However, a long duration between precession pulses results for low nutation levels and, thus, stability is not degraded.

Two methods of applying the precession modulator system are proposed and contrasted in the following. The first method is to have the precession modulator operating continuously for all values of ω_0. At the start of the precession maneuver for this method of application the precession angle starts to increase and the nutation begins to decrease. As the value of ω_0 decreases the increase in precession angle becomes less and less as a result of an increase in the time between allowed precession pulses. In the end result the increase in precession angle will become a function of the nutation build-up due to energy dissipation. A possible example is shown in Figure 9a.

The second method of application is to use the precession modulator only after a threshold level of ω_0 is reached. Initially then, if the value of ω_0 is below this nutation threshold the precession angle will increase at its maximum rate because every

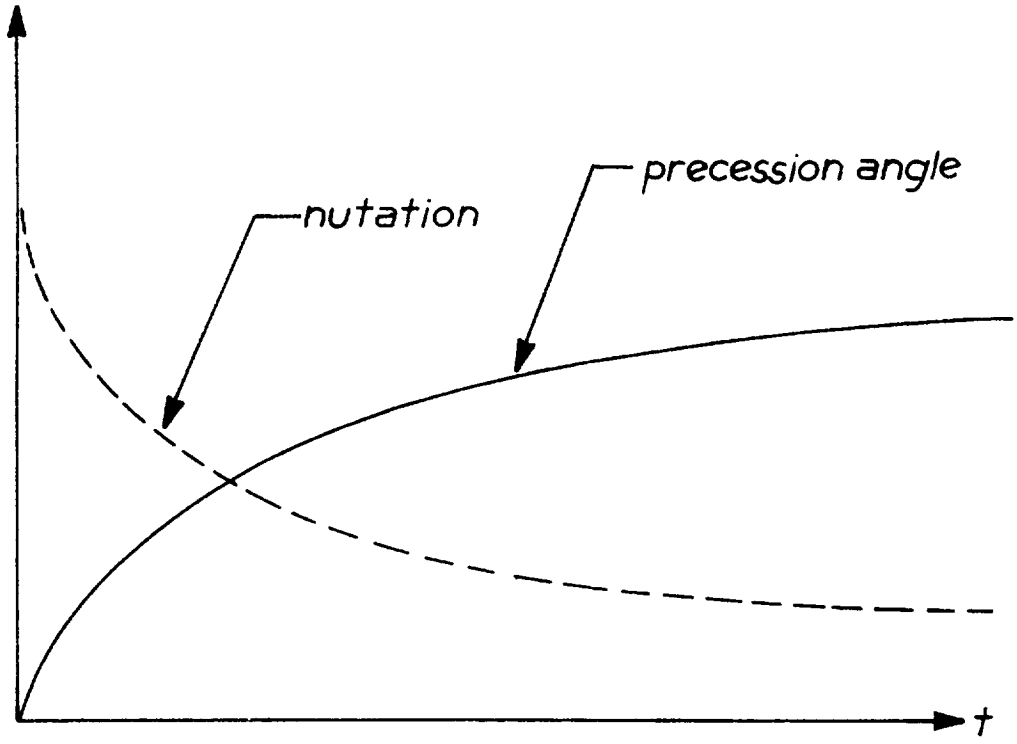

Figure 9a. Continuous Precession Modulation

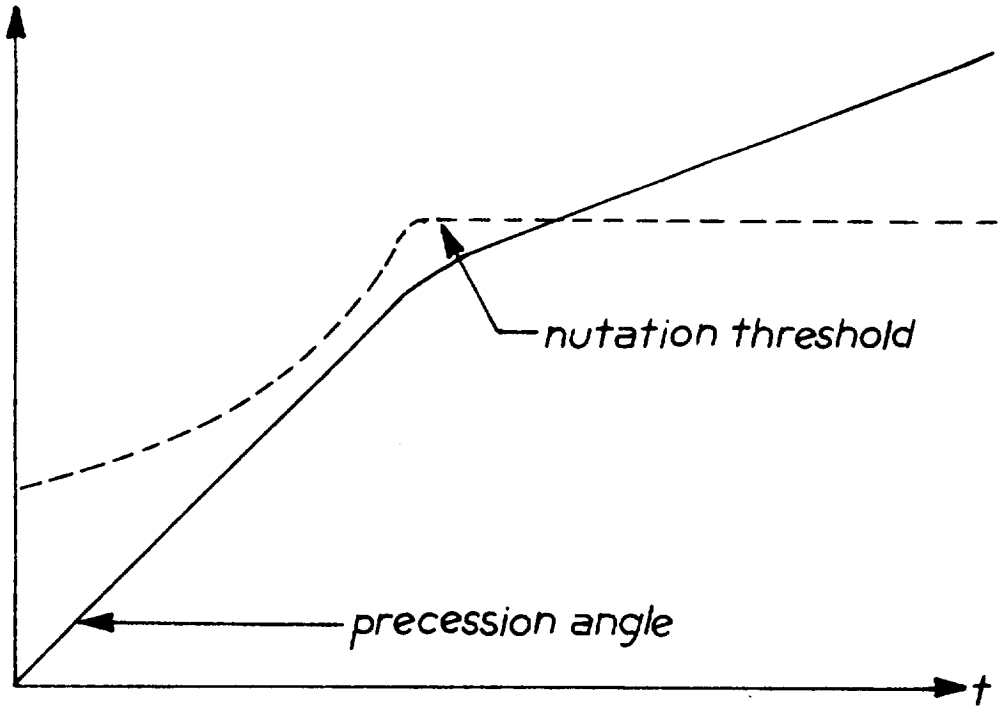

Figure 9b. Modulation After Nutation Threshold

precession pulse will be used. When the threshold value is reached the rate will decrease to some lesser value. A possible example of this method is shown in Figure 9b.

These two methods have the following general results. The first method of continuous operation has the condition that the nutation angle is held to a very low value, but the precession maneuver takes longer. The second method of using the precession modulator only after a nutation threshold is reached has a faster rate of precession angle increase, but operates at a higher nutation level, a level approximately equal to the threshold value.

V. CONCLUSIONS

In this research it has been demonstrated that some form of nutation control is required to be in operation while a precession maneuver is being executed. Three methods of controlling the nutation were examined.

The first method consisted of a thruster command signal being derived from the precession control signal ORed with the output of a separate nutation control system. Digital simulation has shown this method to be the fastest of the three in attaining the final precession angle position. It does so, however, through increased system complexity and hence a possible reduction in reliability.

The other two methods are related to each other in that they both use a modulated precession thrust pulse sequence to control the nutation. This research has demonstrated that precession pulses can also be used to control nutation if they are selected properly. This dual use of the precession pulses creates a simpler system because no separate nutation control system is needed. The first of these precession modulator methods has the modulator acting continuously. This method keeps the nutation level very low, but it also takes a much longer time to execute the precession maneuver. The third method which is also a precession modulator type, uses the modulator only after a specific nutation threshold is reached. This method is only fractionally slower than the separate nutation control system method and is still of the simpler

precession modulator type. The nutation threshold level used in this third method directly affects the time required to complete the precession maneuver. As the nutation threshold is adjusted to higher acceptable levels the precession modulator acts less frequently and modulated precession sequence total time approaches that of the minimum time seen for a completely unmodulated precession sequence.

In the digital simulations conducted using these methods a relatively small value for τ, the energy dissipation time constant was used. This short time for τ necessarily limits the value of the nutation threshold to a low value.

For a precession modulator method, if the threshold level were set too high such that the nutation control due to the precession pulses could not contain the nutation build-up due to energy dissipation, the system would go unbounded just as if no attempt were being made to control the nutation build-up. Future study in this area of longer time constants for the energy dissipation can lead to an increased capability in determining just where the nutation threshold level can be set to avoid a problem such as the one mentioned above. Furthermore, the methods proposed above do not have any actual hardware implementation. The next step in that area is to generate such hardware systems as based upon the comprehensive theoretical analysis presented above which has been extensively verified through the use of digital simulation.

BIBLIOGRAPHY

1. Grasshoff, L. H., "An Onboard, Closed-Loop, Nutation Control System for a Spin-Stabilized Spacecraft", Journal Spacecraft and Rockets, pp. 530-535, May 1968.

2. Taylor, J. M., "The SAS-D Nutation Control System", NASA Technical Document X-732-72-196, Goddard Space Flight Center, Greenbelt, Maryland, June 1972.

3. Taylor, J. M., "Nutation During Precession of a Spin-Stabilized Spacecraft", NASA Technical Document X-732-72-278, Goddard Space Flight Center, Greenbelt, Maryland, August 1972.

APPENDICES

APPENDIX A

Graphical Determination of ϕ_0

Figure 1 of the text shows that $\omega(t_1)$ is a vector sum. In Figure 2 the circle A is the locus of the tip of vector $\omega(t_1)$ as the precession lobe vector is held constant and the vector $\omega(t_0)$ is allowed to assume all possible angular values (i.e., circle A is the result of $\omega(t_1)$ as a function of ϕ_0). The following gives a graphical method for determining the angle ϕ_0 for any vector $\omega(t_1)$ from a drawing similar to Figure 2. The method is simply to calibrate the two circles as to angular displacement. Circle B is marked off in a clockwise direction (the direction of rotation of $\omega(t_0)$) from the ω_y axis which is the zero angle reference. These angles are the values of ϕ_0. The circle A is similarly marked off in a clockwise direction except that the zero reference line is shifted clockwise from a line parallel to the ω_y axis by an angle equal to $\Delta\phi$. The angle $\Delta\phi$ is the angular duration of the precession pulse in terms of nutation circle angular measure. The angle ϕ_0 for any $\omega(t_1)$ can now be read directly from the calibration on circle A. If the vector $\omega(t_0)$ is desired, it can then be obtained by drawing a radial line from the center of circle B to that point on circle B which is marked for the determined value of ϕ_0. This graphical technique can be used to obtain the answer to equation (54) in the text for example.

An example follows in which the angles ϕ_0 for which $|\omega(t_1)| = \omega_0$ are determined. The values of ϕ_0 for which the above condition is satisfied are 29^0 and 239^0 and the two $\omega(t_0)$ vector are shown labeled as such.

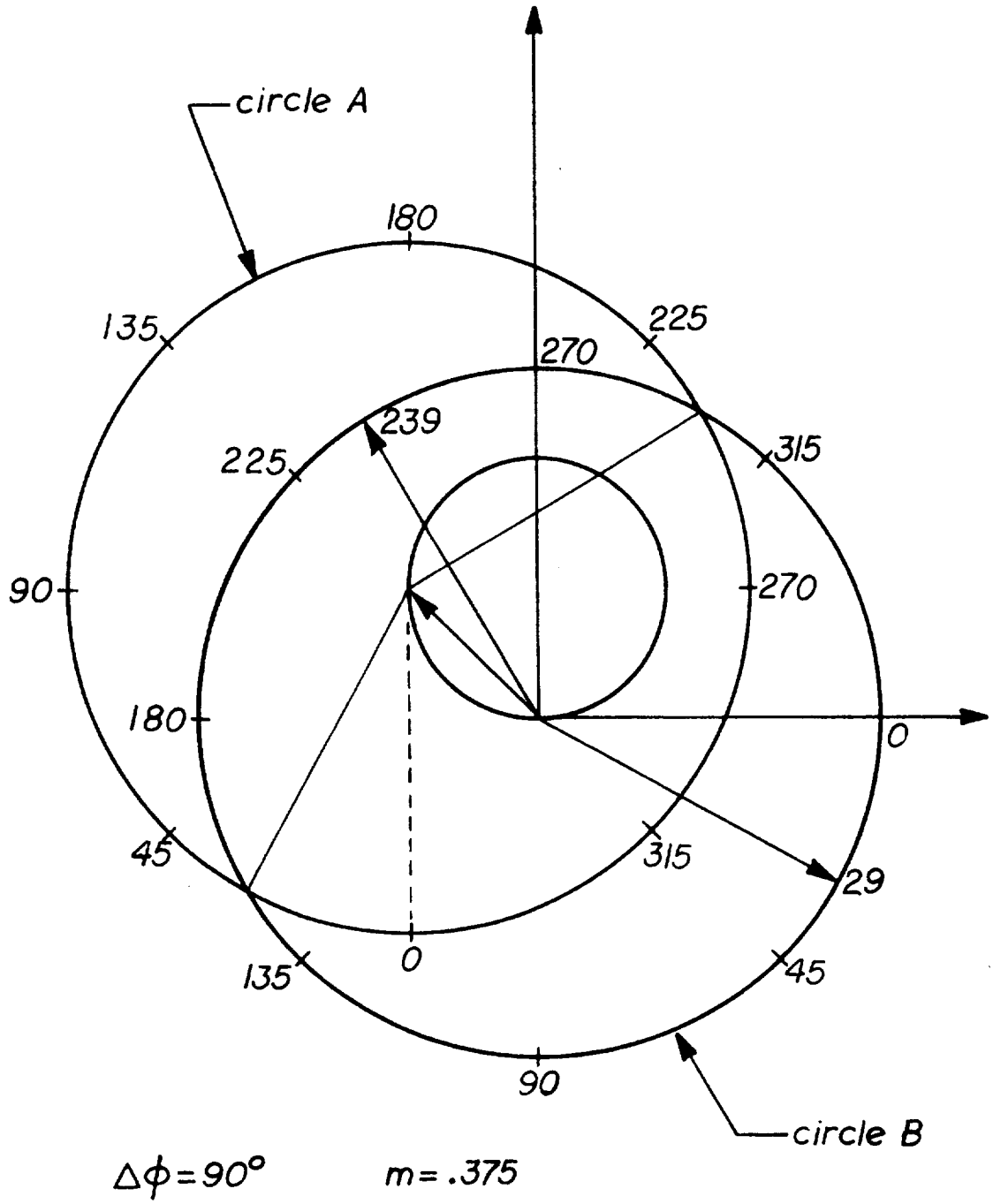

Figure A1. Graphical Determination of ϕ_o

APPENDIX B

Digital Computer Simulation for an SMS Spacecraft Configuration

This appendix provides the results of digital simulation of the nutation-precession control analysis described earlier. An SMS (Synchronous Meteorological Satellite) configuration with relatively short energy dissipation time constant is used. The configuration description is as follows:

SMS Spacecraft Configuration

Mass Properties

Mass = 42.8 Slugs

I_x = 244.4 Slug-Feet^2

I_y = 246.9 Slug-Feet^2

I_z = 97.3 Slug-Feet^2

σ = 0.6039

Angular Velocity

ω_z = 90 RPM (spin axis angular velocity)

Ω = 5.6916 rad/sec (nutation frequency)

Thruster Properties

Thrust = 5 lbs.

Moment Arm = 3 Feet

Duty Cycle = 1/12 seconds (45° of spin period) for Precession

= 0.552 seconds (1/2 nutation period) for Nutation

Energy Dissipation Time Constant

τ = 180 seconds

Results include simulation of the following nutation-precession control laws which are displayed in the referenced figures.

1. Figure B1. Precession Without Nutation Control
2. Figure B2. ORed Precession-Nutation Control
3. Figure B3. Full Modulated Precession (Small Initial Nutation)
4. Figure B4. Full Modulated Precession (Large Initial Nutation)
5. Figure B5. Full Precession-Threshold-Modulated Precession

The above moments of inertia are defined to be consistent with the description of the SMS configuration. This amounts to only a nomenclature change which defines ω_z as the spin axis velocity where as it is defined as ω_x in the text.

In these figures the nutation level is characterized by the dotted line which is the plot of the actual data points generated in the digital simulation. Also included in each figure is the 5.48 mr nutation angle threshold line which gives a quick reference for comparison of the level of nutation during each simulation. The 5.48 mr nutation angle threshold represents the maximum amount of nutation that can be removed by one optimal nutation control thrust pulse.

The correlation between the specific case figures of this appendix and comparable generalized figures in the text is good although exact similarity was not expected. Figure 4b is the

generalization of what is detailed in Figure B1. Both show that as a precession maneuver is carried out without nutation control present the nutation increases rapidly and the direction of the spin axis becomes more unstable. For the case of ORed precession-nutation control, Figures 5b and B2 show that the precession angle increases steadily while the nutation level varies around the nutation angle threshold. Figures B3 and B4 show that the general Figure 9a of the text gives a moderately good description of the results of a continuously modulated precession. The initial value of the nutation is quickly brought down to a low level while the precession angle increase becomes very slow. Finally, it is seen that for the case in which the precession pulse sequence is modulated only after the nutation threshold is reached the slopes of the precession angles of Figure 9b and Figure B5 do not match well. It should be noted, however, that the nutation level in Figure B5 changes value continually which accounts for the numerous changes in slope of the precession angle increase in that figure. What Figures 9b and B5 both show is that once the nutation has passed the threshold level and the precession modulator starts acting that the slope of the precession angle becomes a function of the amount of nutation present.

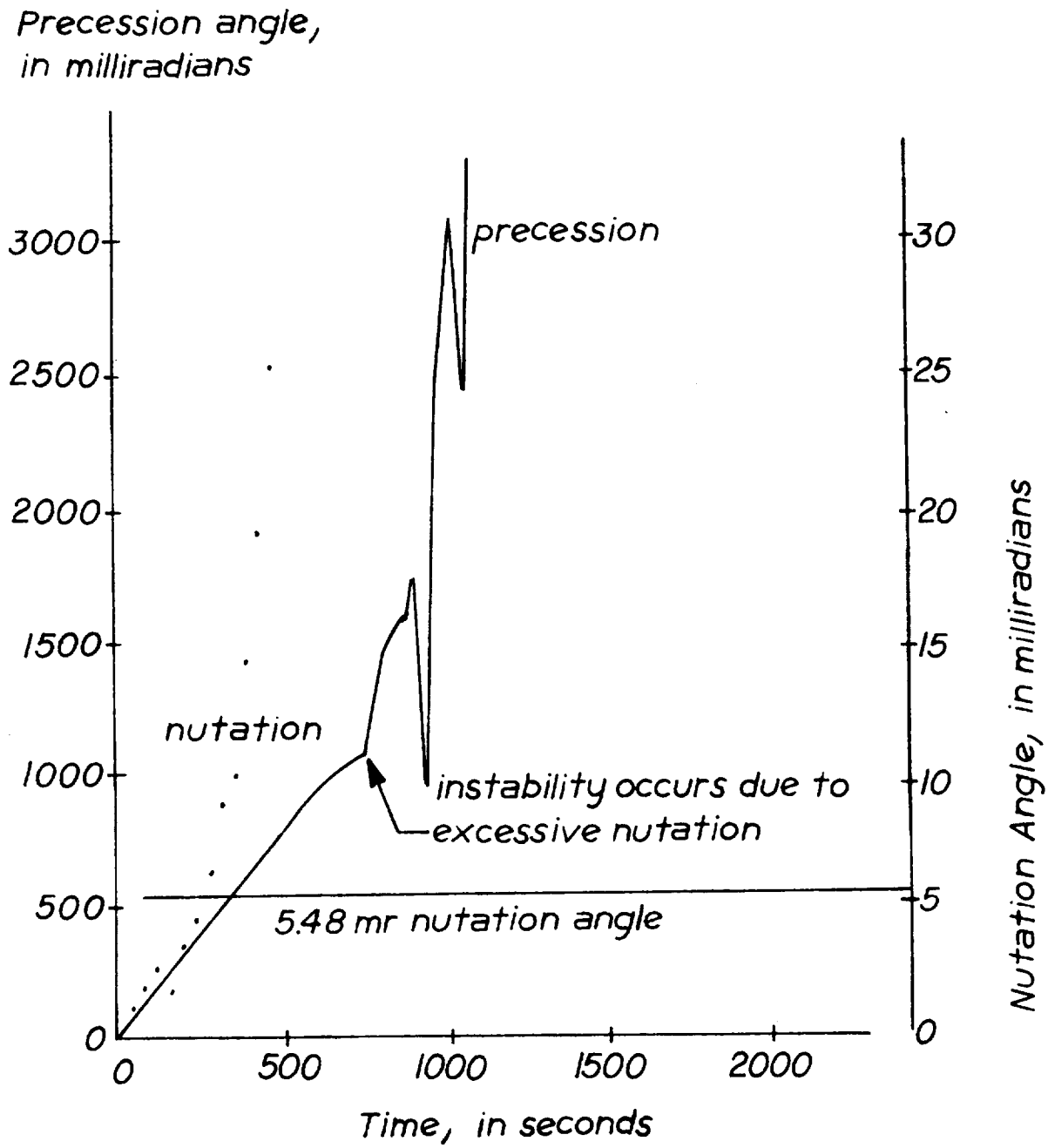

Figure B1. Precession Without Nutation Control

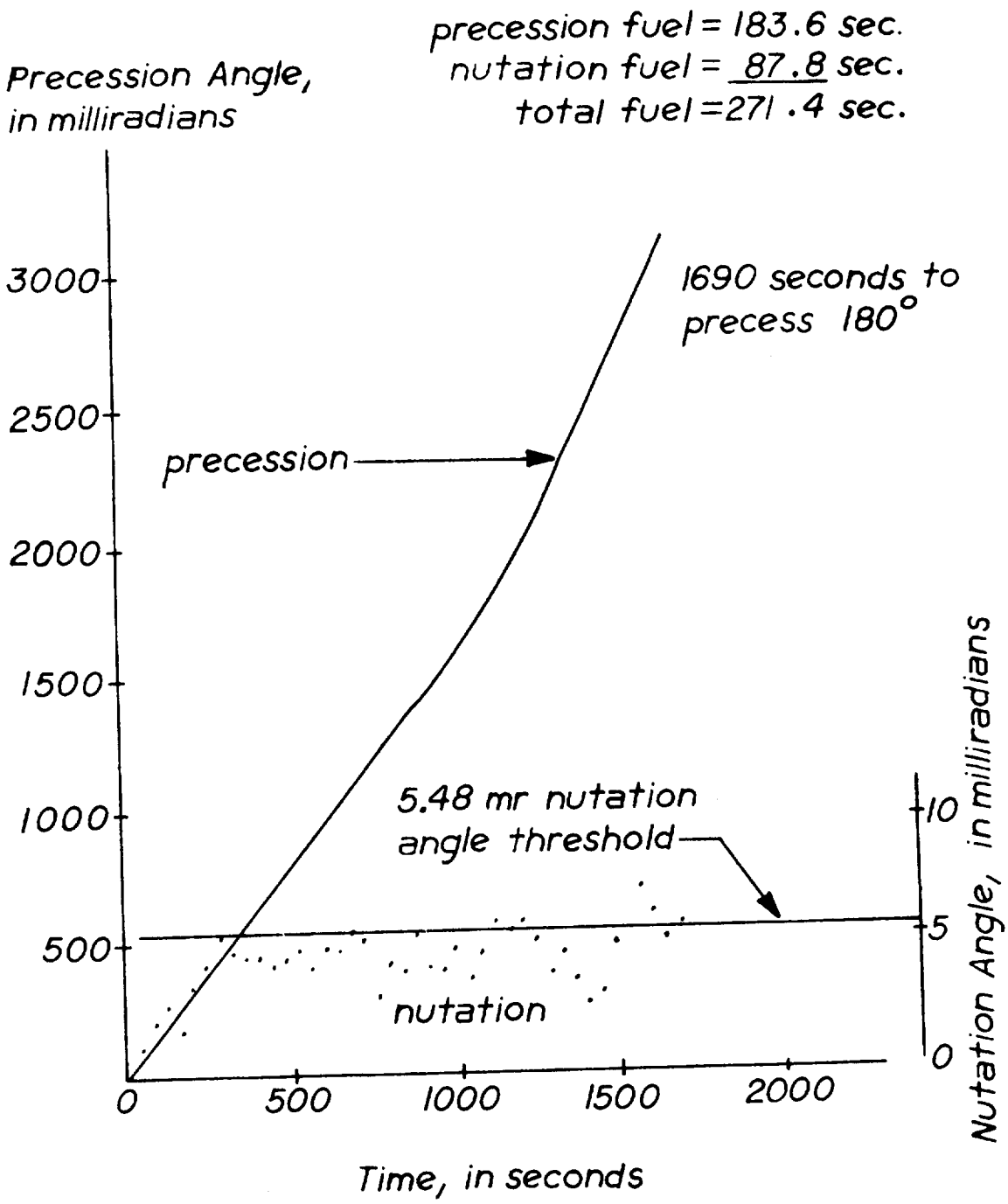

Figure B2. ORed Precession-Nutation Control

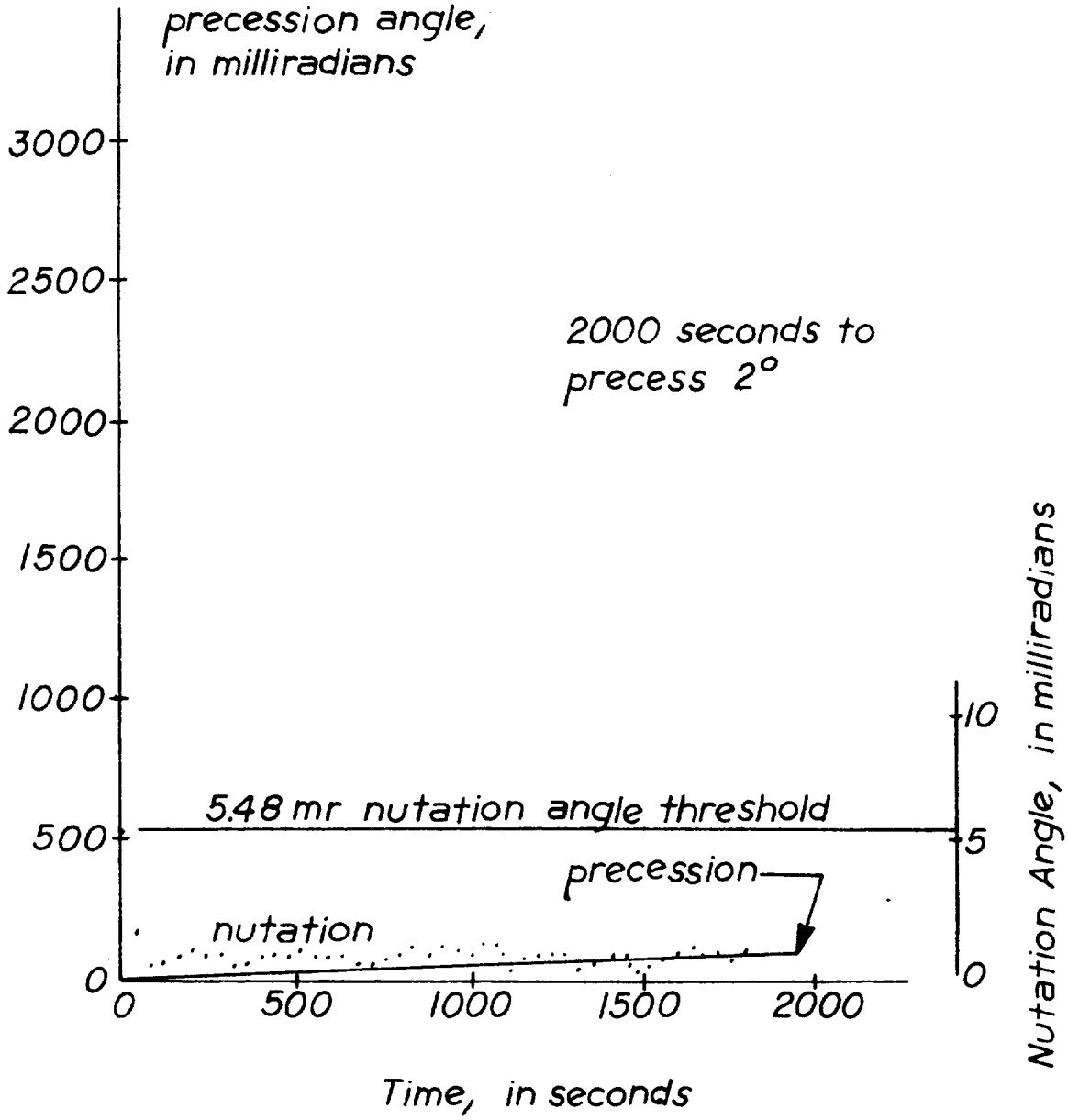

Figure B3. Full Modulated Precession
(Small Initial Nutation)

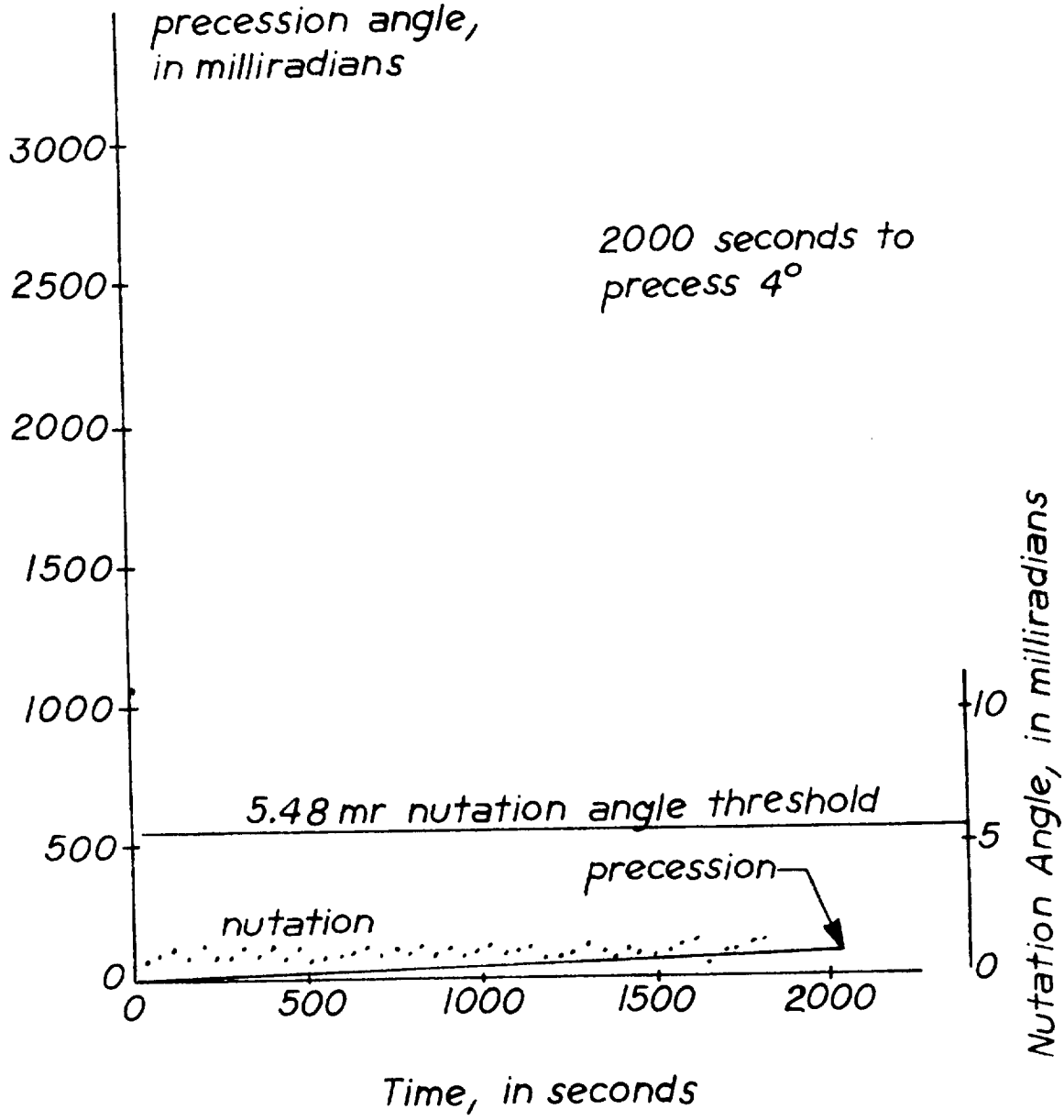

Figure B4. Full Modulated Precession
(Large Initial Nutation)

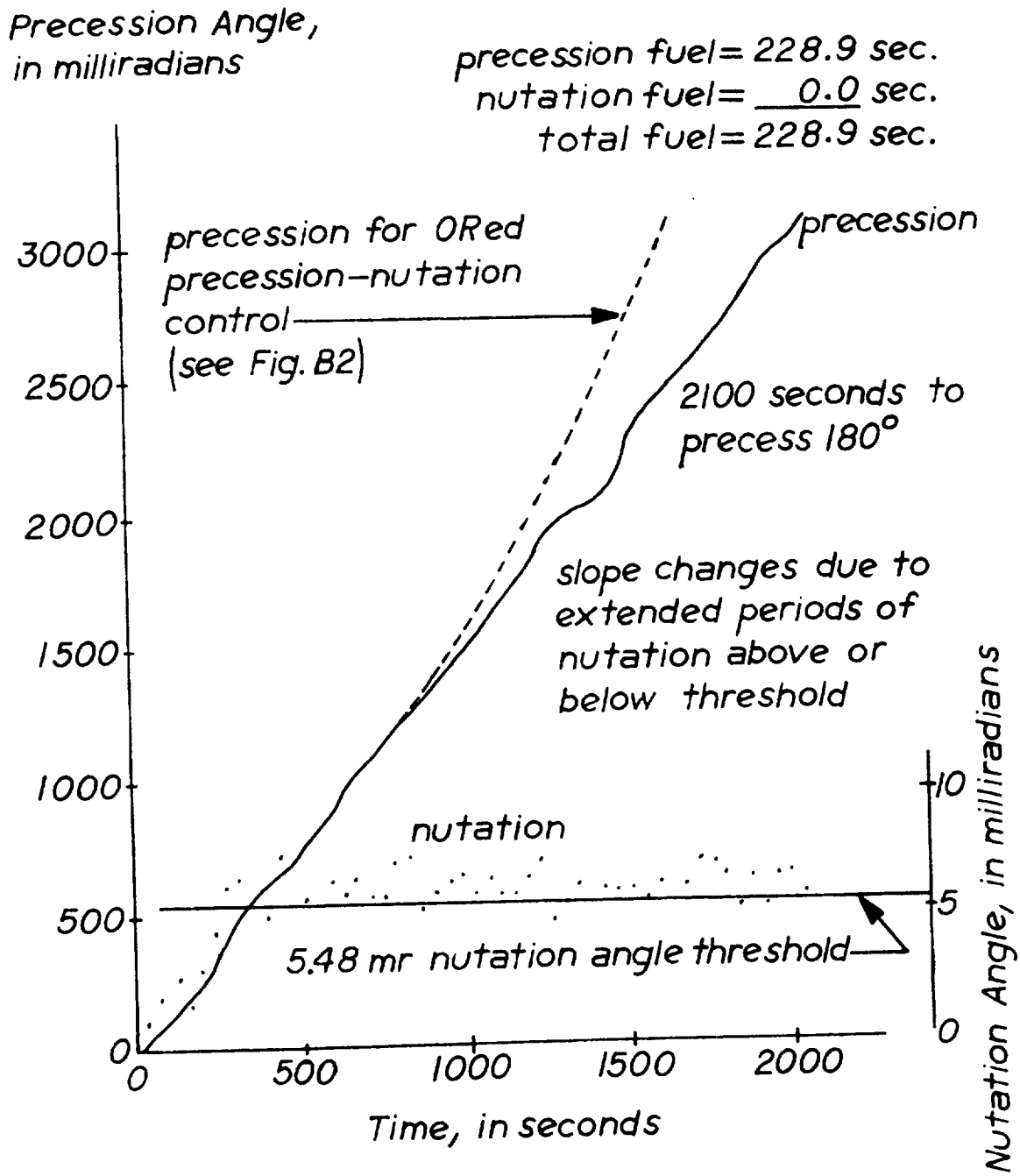

Figure B5. Full Precession-Threshold-Modulated Precession

APPENDIX C

Graphical Solutions to Equation (54)

The figures in this appendix show the effects of changes in the variables m and $\Delta\phi$ upon the range of values that ϕ_0, the solution to $\arccos[-m \sin(\frac{\Delta\phi}{2})]_{II} - \lambda - \frac{\Delta\phi}{2} \leq \phi_0 \leq \arccos[-m \sin(\frac{\Delta\phi}{2})]_{III} - \lambda - \frac{\Delta\phi}{2}$, can take on. The value of λ is held at π radians on all figures. The solution for ϕ_0 on the figures for the above equation is the area(s) marked with the symbol "ϕ_0". The vertical distance between the solution limit curves which bound ϕ_0 is the angle ℓ as described in Figure 8 and equation (55) of the text. The conclusion of this appendix is that for $m > 1$ the duration of the thrust pulse, $\Delta\phi$, is restricted to less effective lengths of time.

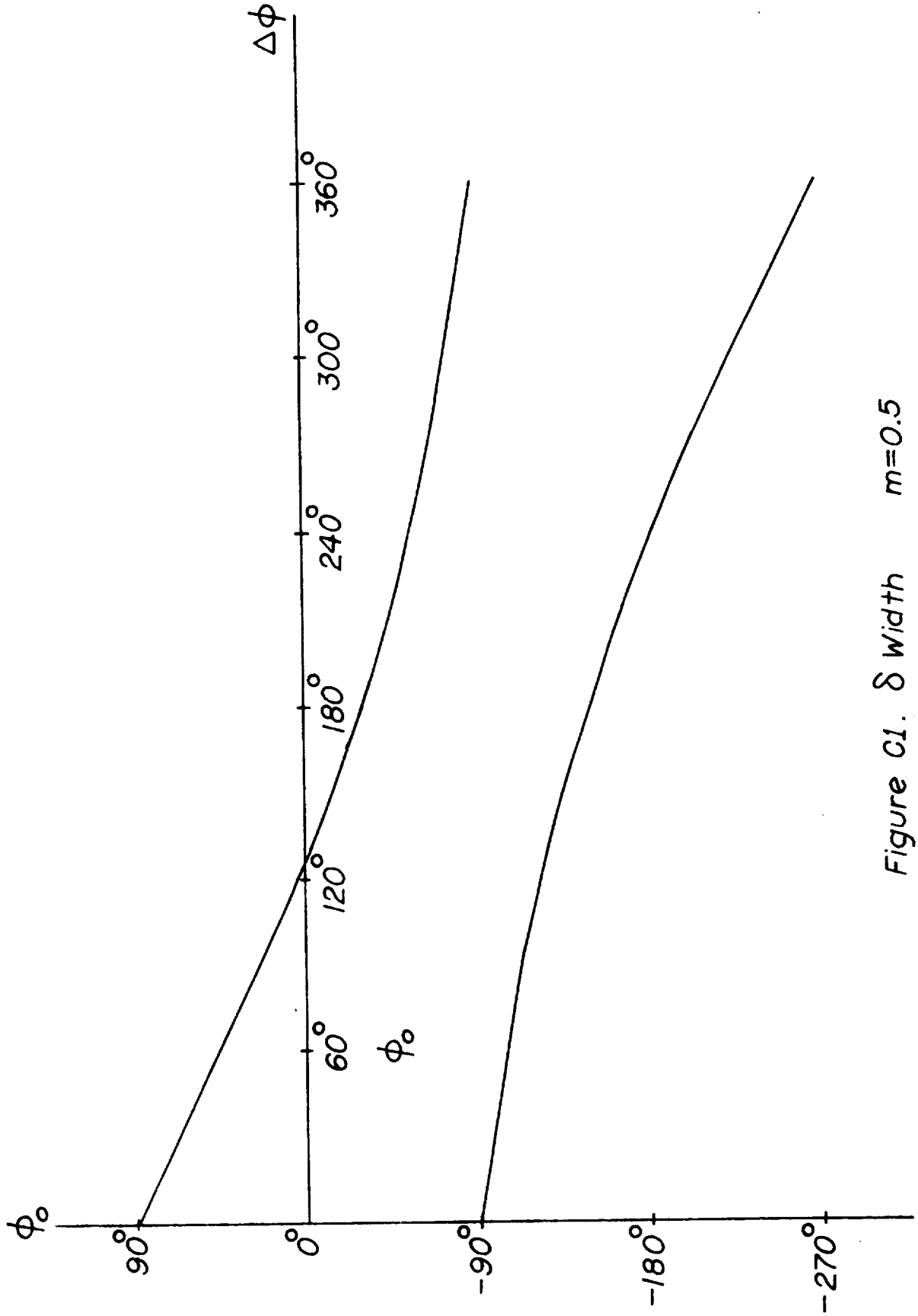

Figure 01. δ Width m=0.5

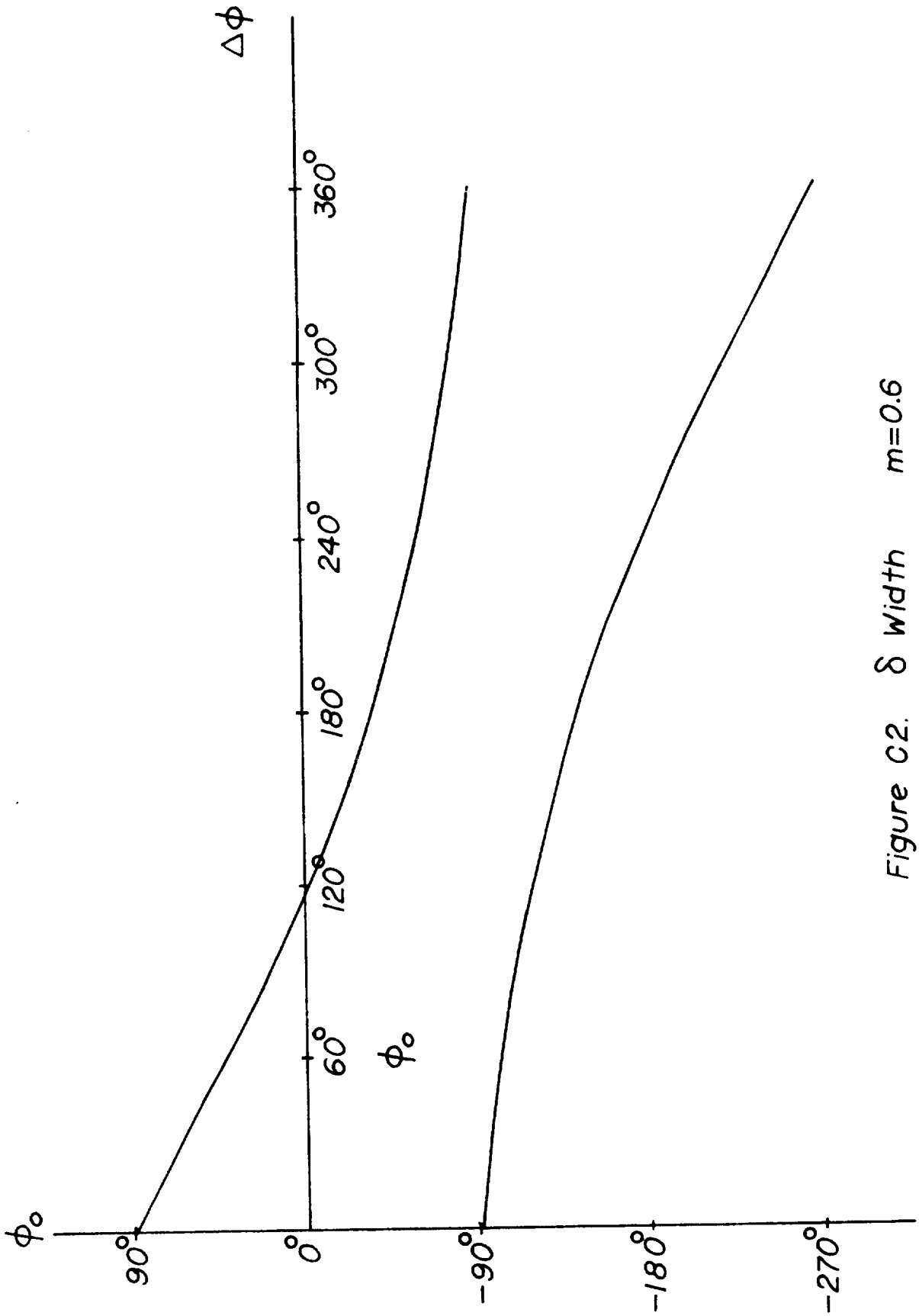

Figure C2. δ Width m=0.6

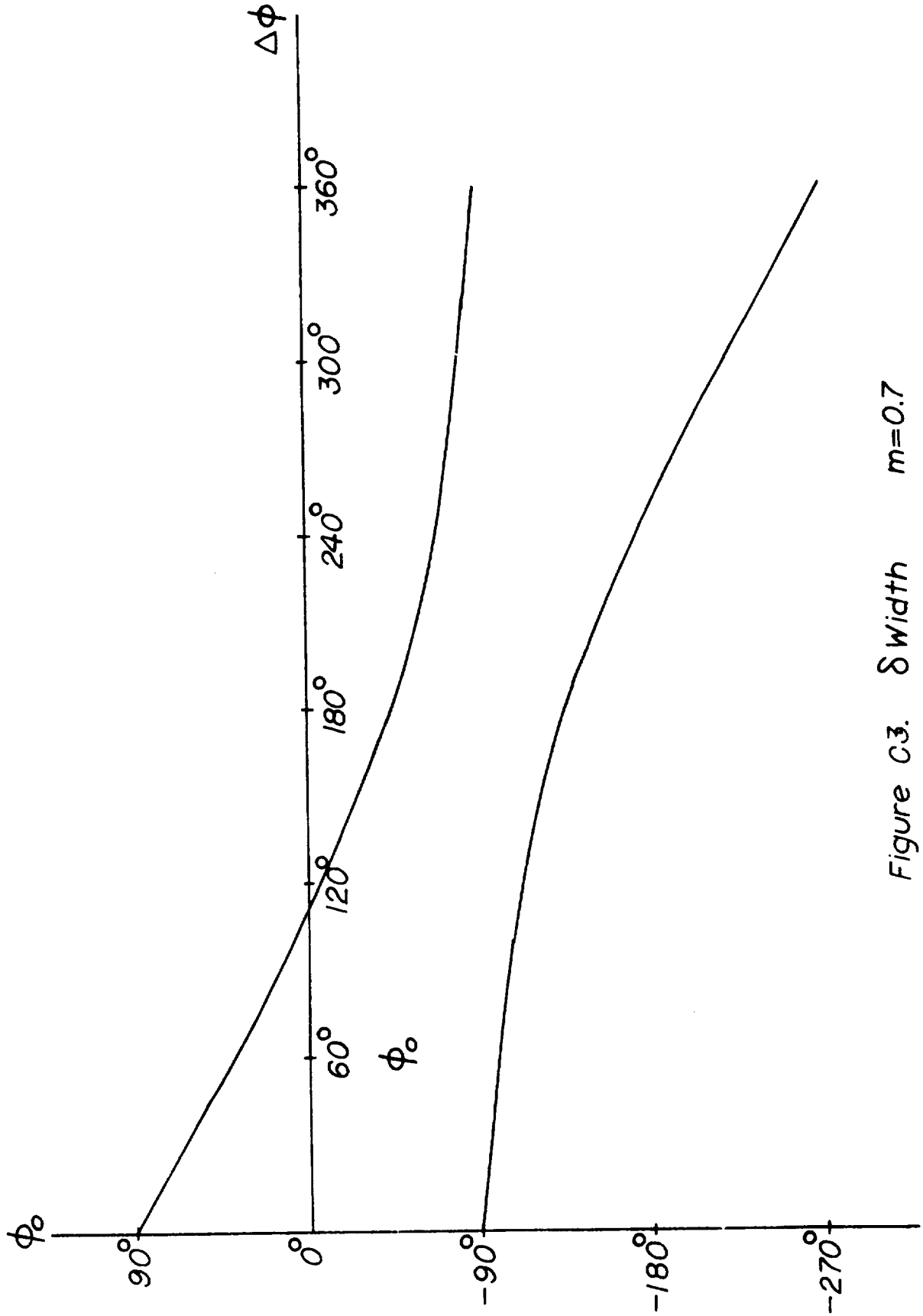

Figure C3. δ Width m=0.7

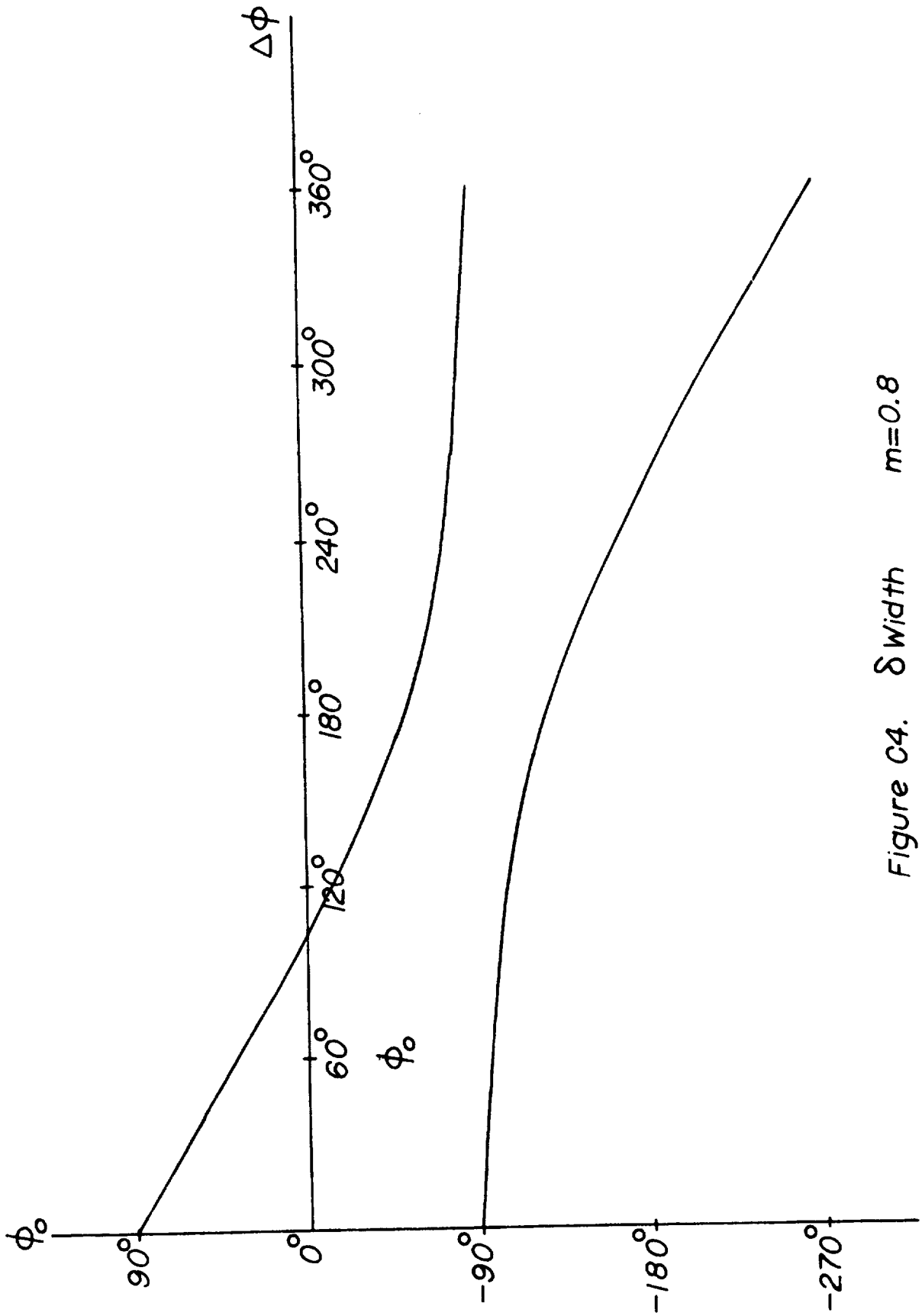

Figure C4. δ Width m=0.8

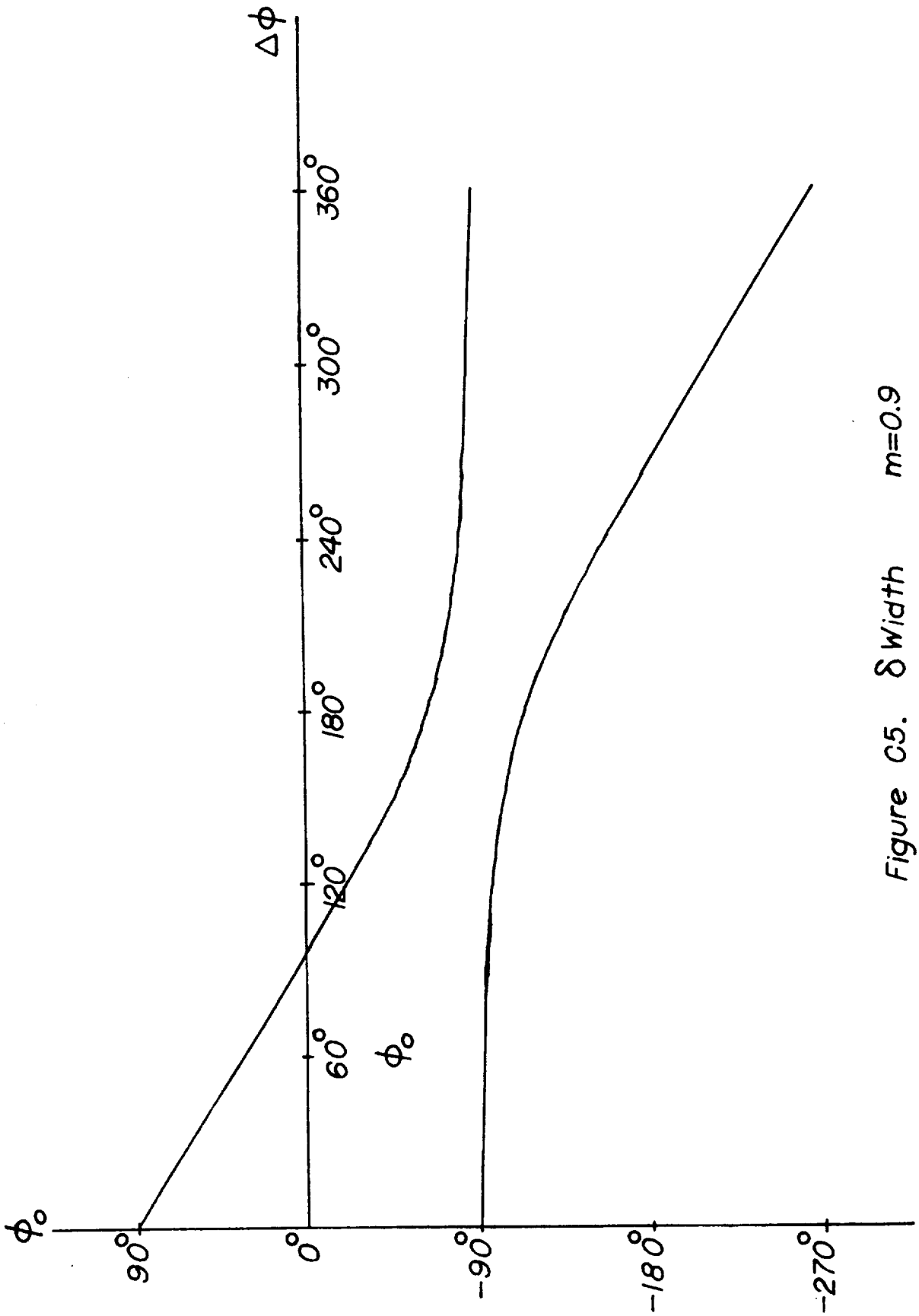

Figure 05. δ Width m=0.9

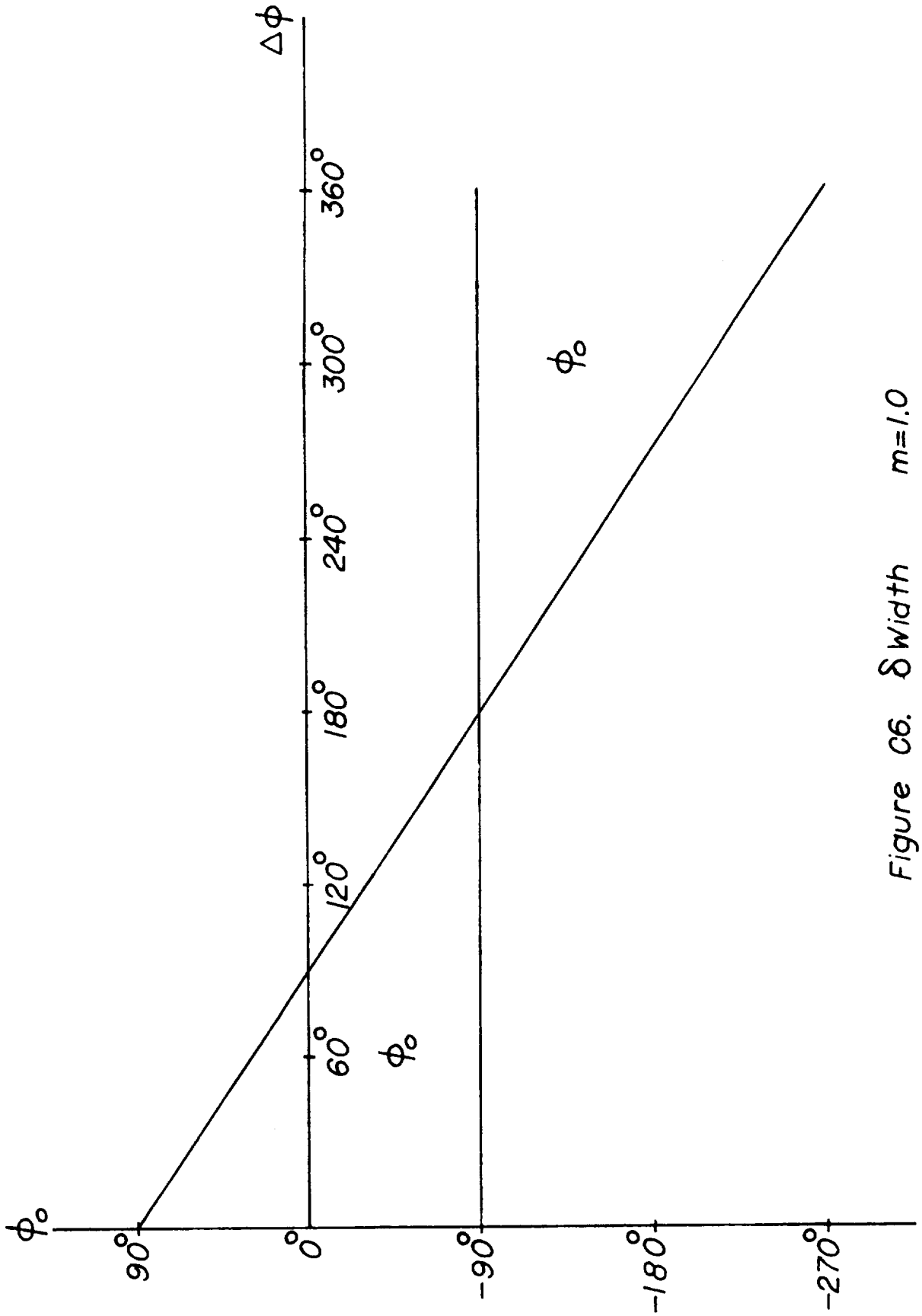

Figure C6. δ Width m=1.0

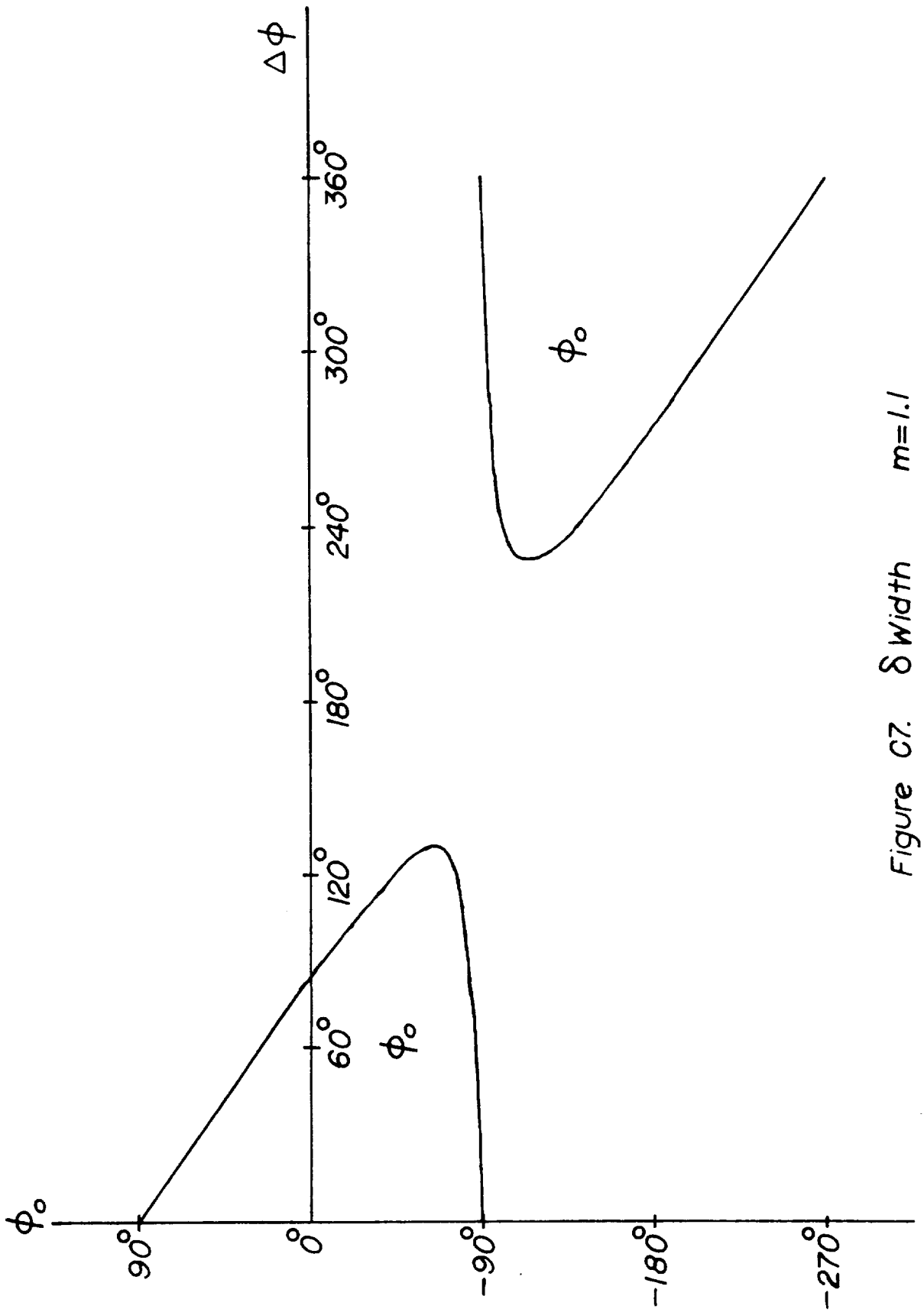

Figure C7. δ Width m=1.1

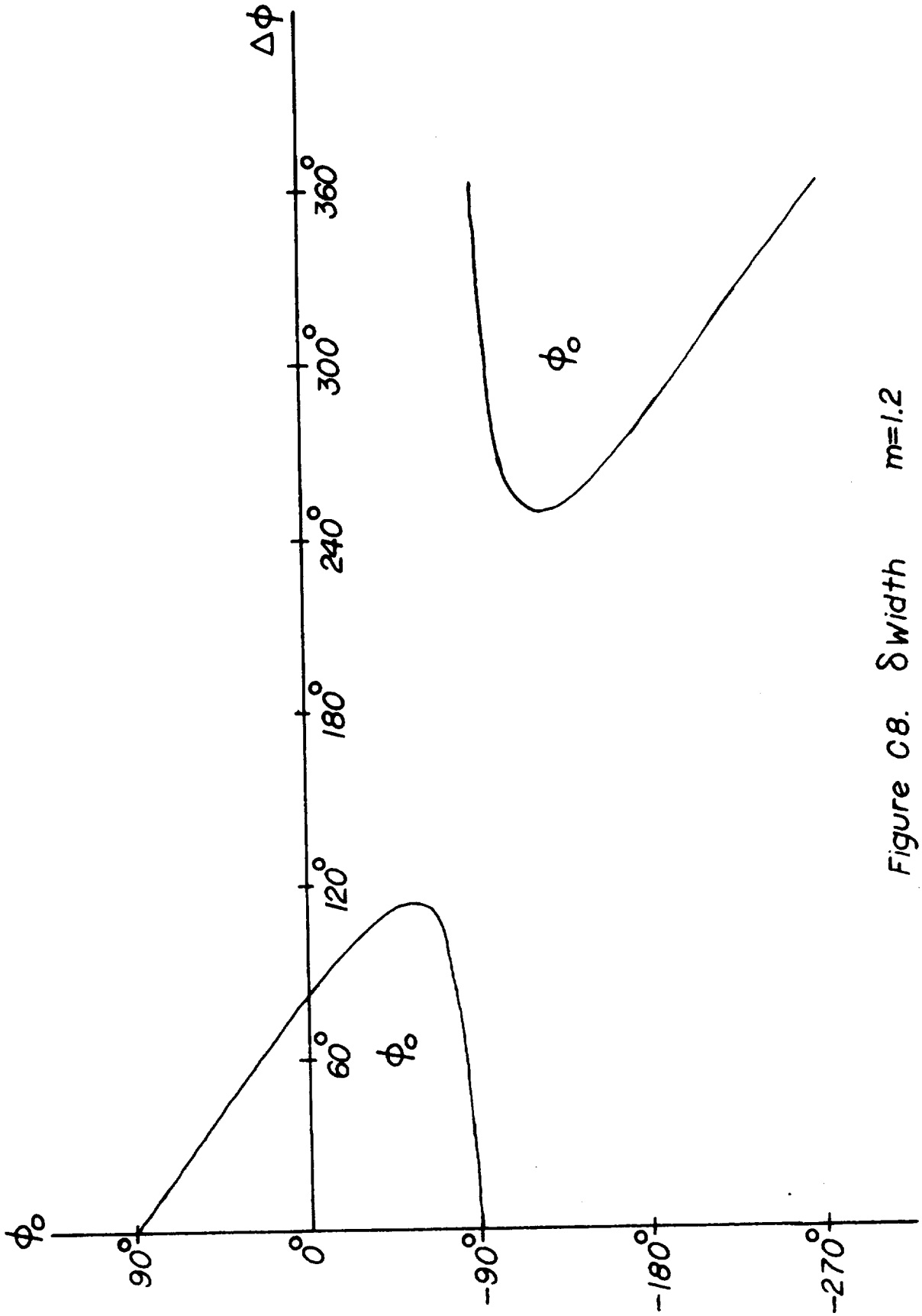

Figure C8. δ width m=1.2

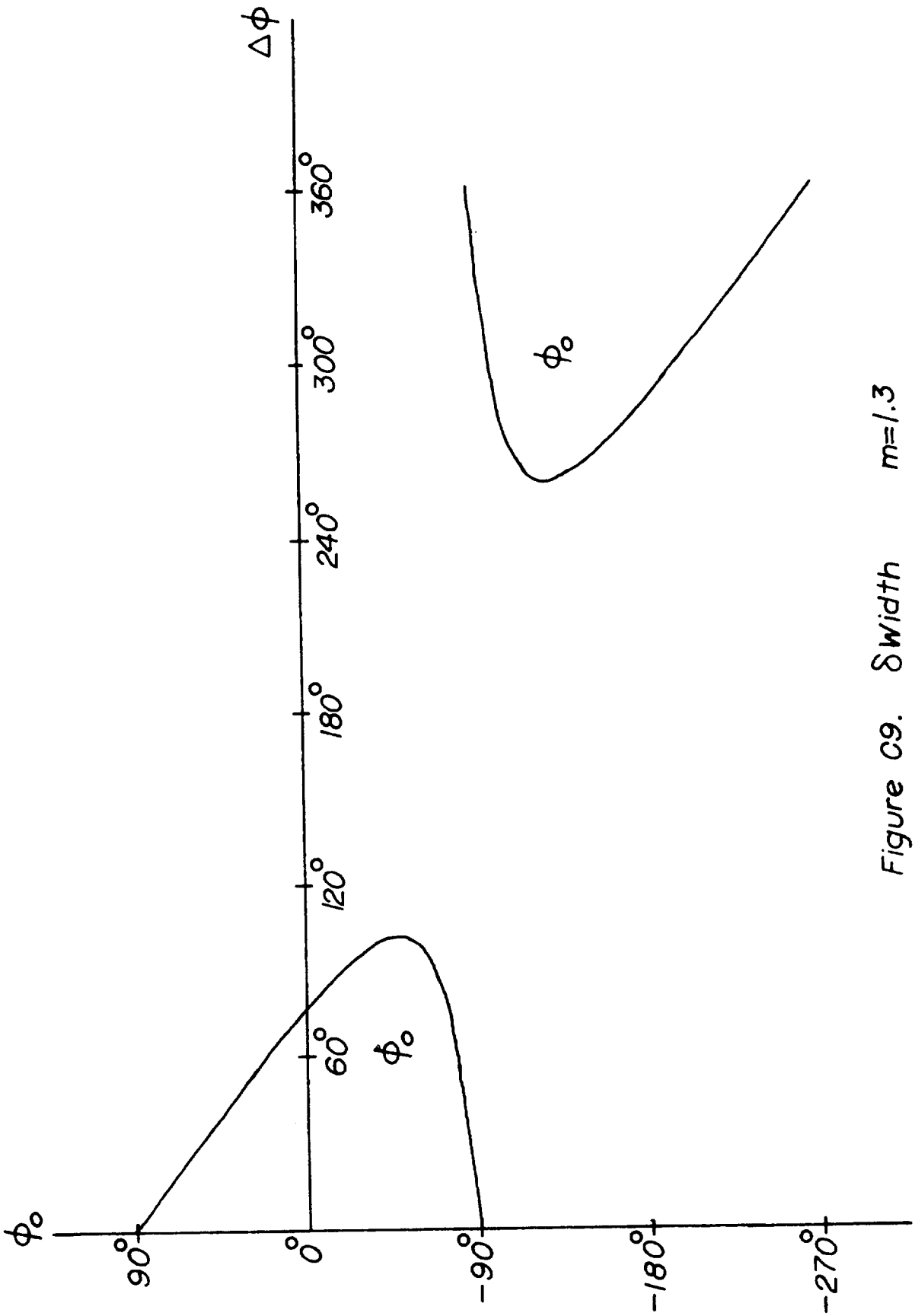

Figure C9. δ Width m=1.3

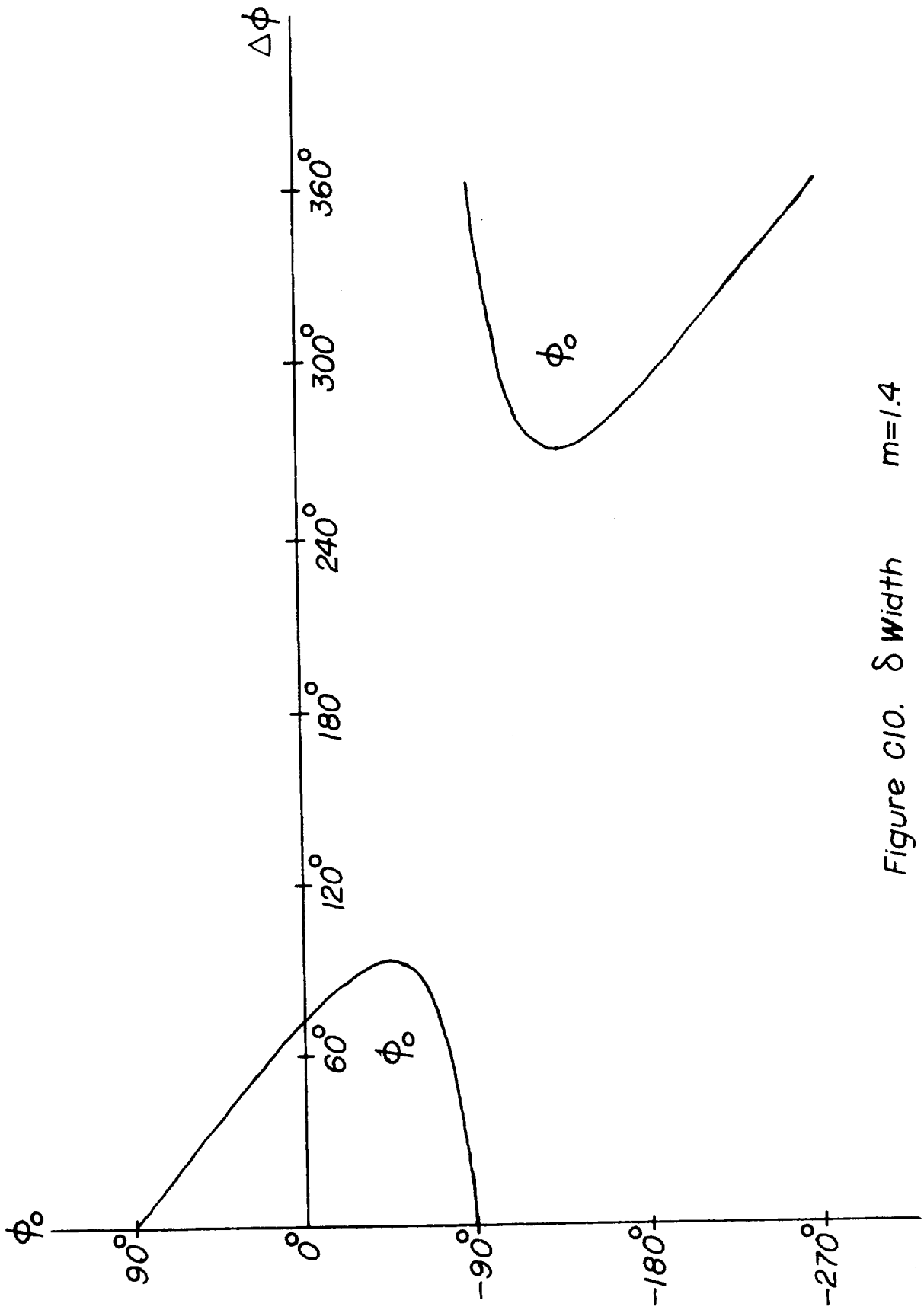

Figure C10. δ Width m=1.4

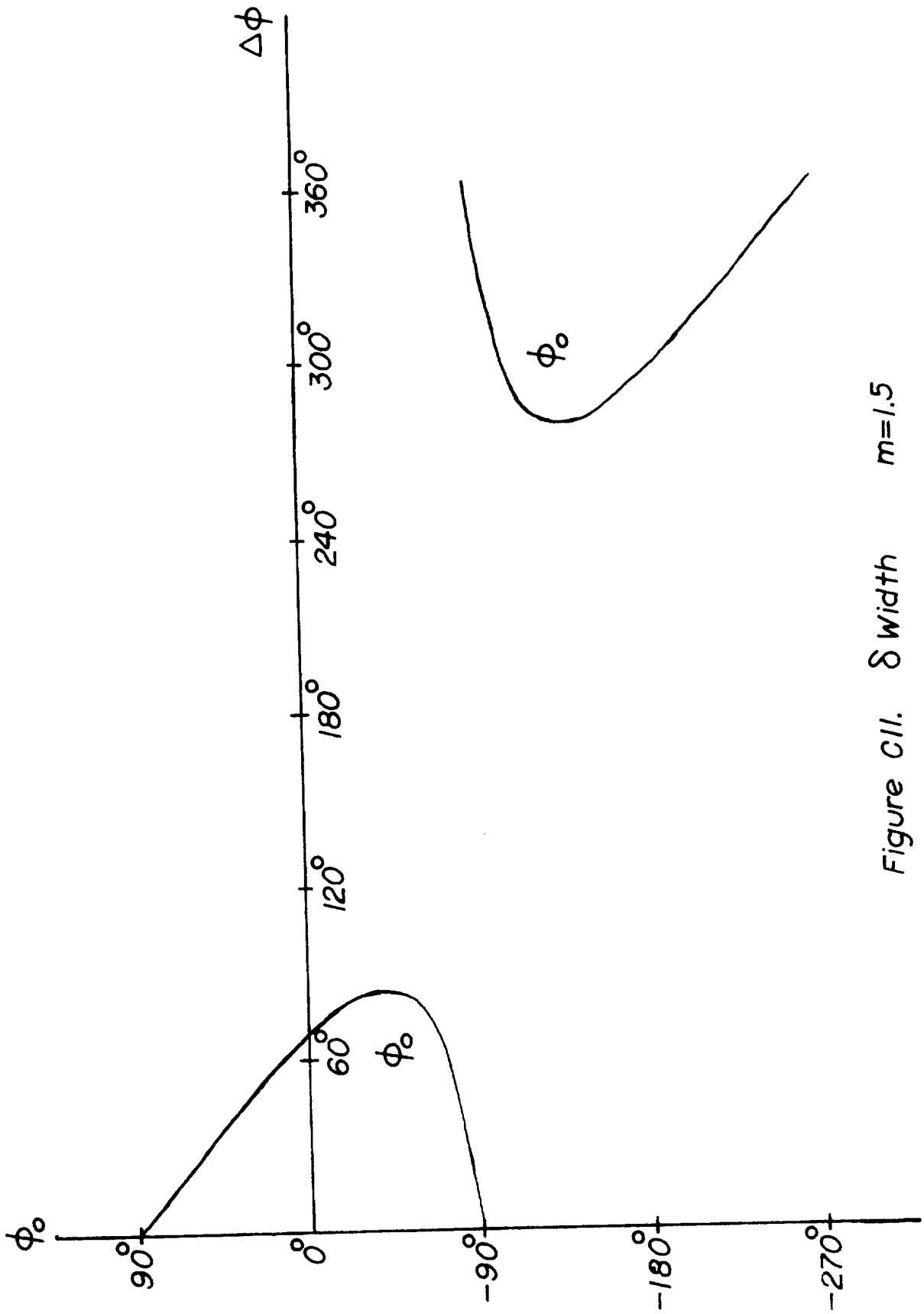

Figure C11. δ Width m=1.5

APPENDIX D

Development of the Complex Differential Equation Describing the Transverse Angular Velocity

In this appendix a brief development of the complex differential equation describing the transverse angular velocity is given. Consider the following basic vector equation

$$\dot{\underline{H}} = \underline{M} \tag{D1}$$

where $\underline{H}$ is the total angular momentum and $\underline{M}$ is the total applied torque relating to a spacecraft. In terms of a Newtonian coordinate system and a spacecraft fixed coordinate system that rotates with respect to the Newtonian system the above equation is rewritten in terms of these coordinate systems.

$$\dot{\underline{H}}_N = \dot{\underline{H}}_R + \underline{\omega} \times \underline{H}_N \tag{D2}$$

where $\underline{\omega}$ is the angular velocity between those systems. In terms of the total inertia $\underline{I}$ and $\underline{M}$ this becomes

$$\underline{I}\,\dot{\underline{\omega}} + \underline{\omega} \times (\underline{I}\,\underline{\omega}) = \underline{M} \tag{D3}$$

Expansion into the scalar equations gives

$$\begin{aligned} I_x\dot{\omega}_x + (\omega_y I_z \omega_z - \omega_z I_y \omega_y) &= M_x \\ I_y\dot{\omega}_y + (\omega_z I_x \omega_x - \omega_x I_z \omega_z) &= M_y \\ I_z\dot{\omega}_z + (\omega_x I_y \omega_y - \omega_y I_x \omega_x) &= M_z \end{aligned} \tag{D4}$$

The x axis is the spin axis and $\dot{\omega}_x = 0$ is assumed. The remaining differential equations are rewritten as

$$\dot{\omega}_y - \frac{\omega_x}{I_y}(I_z - I_x)\omega_z = \frac{M_y}{I_y}$$

$$\dot{\omega}_z + \frac{\omega_x}{I_z}(I_y - I_x)\omega_y = \frac{M_z}{I_z} \tag{D5}$$

or

$$\dot{\omega}_y - \Omega_y \omega_z = N_y$$

$$\dot{\omega}_z + \Omega_z \omega_y = N_z \tag{D6}$$

where

$$\Omega_y = \frac{\omega_x}{I_y}(I_z - I_x), \quad \Omega_z = \frac{\omega_x}{I_z}(I_y - I_x)$$

$$N_y = \frac{M_y}{I_y}, \quad N_z = \frac{M_z}{I_z} \tag{D7}$$

Now by using complex variables notation the equations of (D6) can be written as

$$\dot{\omega}(t) + i\Omega\omega(t) = N \tag{D8}$$

where

$$\omega(t) = \omega_y(t) + i\left(\frac{\Omega_y}{\Omega_z}\right)^{1/2} \omega_z(t),$$

$$\Omega = (\Omega_y \Omega_z)^{1/2}, \tag{D9}$$

and

$$N = N_y + i\left(\frac{\Omega_y}{\Omega_z}\right)^{1/2} N_z.$$

Equation (D8) is the same as equation (1) in the text.